DOI: 10.1002/ar.24827

WILEY

SPECIAL ISSUE ARTICLE

Cranial functional morphology of the pseudosuchian Effigia and implications for its ecological role in the Triassic

Accepted: 7 October 2021

Jordan Bestwick¹ | Andrew S. Jones¹ | Sterling J. Nesbitt² | Stephan Lautenschlager¹ | Emily J. Rayfield³ | Andrew R. Cuff⁴ David J. Button⁵ | Paul M. Barrett⁵ | Laura B. Porro⁶ | Richard J. Butler¹

Correspondence

Jordan Bestwick, School of Geography, Earth and Environmental Sciences, University of Birmingham, Edgbaston, Birmingham B15 2TT, UK. Email: jordan.bestwick92@gmail.com

Funding information

National Science Foundation, Grant/ Award Number: EAR 1943286; Leverhulme Trust, Grant/Award Number: RPG-2019-364

Abstract

Pseudosuchians, archosaurian reptiles more closely related to crocodylians than to birds, exhibited high morphological diversity during the Triassic with numerous examples of morphological convergence described between Triassic pseudosuchians and post-Triassic dinosaurs. One example is the shuvosaurid Effigia okeeffeae which exhibits an "ostrich-like" bauplan comprising a gracile skeleton with edentulous jaws and large orbits, similar to ornithomimid dinosaurs and extant palaeognaths. This bauplan is regarded as an adaptation for herbivory, but this hypothesis assumes morphological convergence confers functional convergence, and has received little explicit testing. Here, we restore the skull morphology of Effigia, perform myological reconstructions, and apply finite element analysis to quantitatively investigate skull function. We also perform finite element analysis on the crania of the ornithomimid dinosaur Ornithomimus edmontonicus, the extant palaeognath Struthio camelus and the extant pseudosuchian Alligator mississippiensis to assess the degree of functional convergence with a taxon that exhibit "ostrich-like" bauplans and its closest extant relatives. We find that Effigia possesses a mosaic of mechanically strong and weak features, including a weak mandible that likely restricted feeding to the anterior portion of the jaws. We find limited functional convergence with Ornithomimus and Struthio and limited evidence of phylogenetic constraints with extant pseudosuchians. We infer that Effigia was a specialist herbivore that likely fed on softer plant material, a niche unique among the study taxa and potentially among contemporaneous Triassic herbivores. This study increases the known functional diversity of pseudosuchians and highlights that superficial morphological similarity between unrelated taxa does not always imply functional and ecological convergence.

KEYWORDS

convergence, Effigia, functional morphology, herbivory, Ornithomimus, pseudosuchian, Struthio, Triassic

¹School of Geography, Earth and Environmental Sciences, University of Birmingham, Birmingham, UK

²Department of Geosciences, Virginia Tech, Blacksburg, Virginia, USA

³School of Earth Sciences, University of Bristol, Bristol, UK

⁴Centre for Anatomical and Human Sciences, Hull York Medical School, University of York, York, UK

⁵Department of Earth Sciences, The Natural History Museum, London, UK

⁶Centre for Integrative Anatomy, Department of Cell and Developmental Biology, University College London, London, UK

1 | INTRODUCTION

The Triassic Period was a key time in evolutionary history that witnessed the emergence and radiation of Archosauria, the group of reptiles that includes crocodylians and birds (Butler et al., 2011; Nesbitt, 2003, 2011; Nesbitt et al., 2010). The Late Triassic is considered a highly successful interval for Pseudosuchia-archosaurs more closely related to crocodylians than to birds-as this clade exhibited high levels of morphological diversity during this time (Brusatte et al., 2008, 2010). Numerous instances of morphological convergence have been described between Late Triassic pseudosuchians and distantly related archosaurs, many of which post-date the Triassic (Stocker et al., 2016). Examples include: the large, broad crania of ornithosuchids and rauisuchids, reminiscent of large theropod dinosaurs (Brusatte et al., 2009; Walker, 1964; Weinbaum, 2011, 2013); the quadrupedal, armored bodies of aetosaurs, similar to the body plans of ankylosaurian dinosaurs (Desojo et al., 2013; Stocker et al., 2016); and the elongate rostra and bodies of phytosaurs which are similar to those of extant crocodylians (Chatterjee, 1978; Stocker, 2012; Witzmann et al., 2014). Pseudosuchians were thus among the dominant tetrapods of many Late Triassic food webs and filled a diverse array of ecological roles within terrestrial and semi-aquatic ecosystems (Brusatte et al., 2008).

Another well-known case of morphological convergence is the shuvosaurid poposauroid Effigia okeeffeae from the Late Triassic of southwestern United States (Nesbitt, 2007; Nesbitt & Norell, 2006). Effigia has been described as having a theropod-like body plan due to its gracile morphology, bipedal posture and the way in which its femora articulate with the pelvis (Nesbitt, 2007). More specifically, although all known cranial material of Effigia is partially crushed, reconstructions suggest a remarkable level of cranial convergence with Late Cretaceous ornithomimid dinosaurs, including large cranial fenestrae, enlarged orbits and edentulous jaws that were likely covered with a rhamphotheca (Nesbitt, 2007; Norell et al., 2001; Stocker et al., 2016). A similar cranial morphology is also present in extant palaeognath birds, most notably the ostrich (Struthio camelus) (Zusi, 1993), and, to a lesser extent, the abelisauroid dinosaur Limusaurus from the Late Jurassic (Stocker et al., 2016; Xu et al., 2009). This independent, repeated evolution of an edentulous, bipedal and gracile bauplan (informally referred to as "ostrichlike") not only further highlights the morphological disparity of Late Triassic pseudosuchians but also acts as an example of the extent to which archosaurs repeatedly occupied the same areas of morphospace (Brusatte et al., 2008, 2010; Nesbitt, 2011; Stocker et al., 2016).

An ostrich-like bauplan has been cited as a possible adaptation for herbivory (Barrett, 2005; Makovicky

et al., 2004; Nesbitt, 2007; Osmólska, 1997; Stocker et al., 2016) because extant birds with these features are known to be herbivorous and have been studied in detail (e.g., in Struthio; Williams et al., 1993; Milton et al., 1994). Observational studies are not possible for extinct taxa, but inferences can be made in various ways. Most dietary interpretations of Effigia and ornithomimids come from: (a) comparative morphology of anatomical characters with extant birds such as palaeognaths and Anseriformes (waterfowl) (Barrett, 2005; Nesbitt, 2007; Norell et al., 2001); (b) assessing the evolutionary pathways of cranial eco-functional characters that likely facilitated herbivory (Button & Zanno, 2020; Zanno & Makovicky, 2011); (c) preserved gut contents; and (d) other evidence such as the presence of a gastric mill (Kobayashi et al., 1999; Makovicky et al., 2004). These types of evidence, however, are limited either by the quality of the fossil record or by assumptions on the strength of relationships between morphology and inferred function (Bestwick et al., 2018 and references therein). Quantitative investigations into the degree of functional convergence between Effigia and morphologically similar, but distantly related, archosaurs are thus needed for inferring the likelihood that these taxa performed similar ecological roles.

Few studies have investigated the functional morphology of Triassic pseudosuchians, particularly with regard to potential feeding behaviors. Nevertheless, some valuable insights have been gained into pseudosuchian diets, how these taxa partitioned or competed for resources and on their broader evolution by using various modeling biomechanical methods (Desojo Vizcaíno, 2009; Baczko et al., 2014; Baczko, 2018; Taborda et al., 2021). Two-dimensional muscle reconstructions and lever mechanical modeling of aetosaur jaws, for example, found that some aetosaurs had slow and powerful bites, interpreted as an adaptation for processing tough vegetation, whereas others exhibited faster, weaker bites interpreted as evidence of facultative insectivory (Desojo & Vizcaíno, 2009). Similar techniques found that ornithosuchids were capable of intermediately powerful, slower bites and were thus likely to have occupied a mesopredator and/or scavenger role in Late Triassic food webs (Baczko, 2018). Two-dimensional models are, however, a simplified version of complex threedimensional anatomy and are only capable of modeling jaw function via simple lever mechanics (Anderson et al., 2011; Davis et al., 2010; Kammerer et al., 2006; Porro et al., 2011; Santana, 2016). This is particularly problematic for many archosaur groups, such as extant crocodylians, which can generate high mediolateral forces from their jaw muscles (Porro et al., 2011). By contrast, three-dimensional techniques, such as finite

element analysis (FEA), can more accurately predict the performance of organic structures because they can: (a) predict biomechanical stresses and strains across the whole 3D skull; (b) allow incorporation of soft tissue elements such as rhamphothecae to improve biological realism (Cuff & Rayfield, 2015; Lautenschlager et al., 2013) and; (c) can enable modeling of a wider range of feeding-related behaviors, such as twisting, shaking and pecking (McCurry et al., 2015; Porro et al., 2011; Rayfield, 2011; Taborda et al., 2021; Walmsley et al., 2013). Representative investigations into the functional morphology of *Effigia* can thus help to elucidate the true level of functional convergence between this pseudosuchian and other morphologically-similar members of Avemetatarsalia (archosaurs more closely related to birds than crocodiles).

Here, we restore the original morphology of the crushed and deformed skull of Effigia, perform myological reconstructions and apply 3D FEA to investigate the functional morphology of this Late Triassic pseudosuchian, in order to assess its degree of functional convergence with other taxa that exhibit an ostrich-like bauplan. To achieve the latter aim we used previously published 3D cranial models from the ornithomimid dinosaur Ornithomimus edmontonicus and the palaeognath bird Struthio camelus (Cuff et al., 2015; Cuff & Rayfield, 2015). We also included a cranial dataset from Alligator mississippiensis in order to include an extant and pseudosuchian a morphological (Montefeltro et al., 2020). Finally, we modeled the impacts of different-sized rhamphothecae for our extinct study species and simulated pecking-like behaviors for all taxa in order to provide more stringent tests on the degrees of functional convergence and to better assess whether unrelated ostrich-like taxa performed the same ecological roles.

1.1 | Institutional abbreviations

AMNH, American Museum of Natural History, New York, NY; OUVC, Ohio University Vertebrate Collections, Athens, OH; ROM, Royal Ontario Museum, Toronto, Ontario, Canada; RTMP, Royal Tyrrell Museum of Paleontology, Drumheller, Alberta, Canada.

2 | MATERIALS AND METHODS

2.1 | Specimen information

The holotype of *Effigia okeeffeae* (AMNH FR 30587) was computed tomography (CT) scanned at Stony Brook University Hospital on a GE Systems Lightspeed 16 scanner

with an interslice thickness of 0.625 mm. For full image specifications and post-processing procedures, see Nesbitt (2007). The unretrodeformed dataset can be requested through the AMNH.

For comparisons, we modeled the crania of Struthio, Ornithomimus and Alligator. The Struthio specimen was micro-computed tomography (µCT) scanned at the University of Hull, UK, using a X-Tek HMX 160 scanner. Due to specimen size, it was scanned in two parts (anterior and posterior; 758 slices and 846 slices, with voxel sizes of 0.1594 and 0.1425 mm respectively). Both scan sets were rotated and resampled to the same voxel size (0.1594 mm resolution; see also Cuff et al., 2015). The Ornithomimus specimen (RTMP 1995.110.0001) was scanned along the coronal axis for a total of 420 slices (0.63 mm thickness) with a General Electric (GE) LightSpeed Plus CT scanner (see also Cuff & Rayfield, 2015; Tahara & Larsson, 2011). The Alligator specimen (OUVC 9761) was scanned at O'Bleness Memorial Hospital, Athens, Ohio, using a GE Lightspeed Ultra Multislice CT scanner equipped with the Extended Hounsfield option and a "bow-tie" filter. The specimen was scanned helically at a slice thickness of 625 µm, 120-140 kV and 200-300 mA (see also Witmer & Ridgely, 2008).

Struthio was chosen for comparison as it is the taxon most often used by paleontologists as a reference for inferring palaeognath-like behaviors in extinct taxa (Barsbold & Osmólska, 1990; Ji et al., Osmólska, 1997; Zanno & Makovicky, 2011), and it has also been the subject of several biomechanical studies (Cuff et al., 2015; Rayfield, 2011). For this study, sutures were not separately modeled from the rest of the cranium, producing a model that does not exhibit functional kinesis. We acknowledge that this results in a simplified cranium as sutures are known to alter and modulate stress and strain distributions in many taxa, both at the sutural junction and, in some cases, across the entire cranium (Curtis et al., 2013; Dutel et al., 2021; Herring & Teng, 2000; Jones et al., 2017; Kupczik et al., 2007; Moazen et al., 2009; Rafferty et al., 2003). This simplification was done for several reasons (a) sutures take substantial time and anatomical expertise to model, particularly in Struthio where some cranial sutures may become partially fused as individuals mature (Cuff et al., 2015). Consequently, the degree of sutural fusion is not always clear from CT scans and is difficult to representatively model; (b) sutures represent another level of biological complexity that was avoided to make more general inferences from our results; (c) we can make some post hoc inferences as to how the sutures might alter our results based on other more detailed analyses; (d) our Struthio muscle model is already somewhat hypothetical due to using jaw muscle attachment site from

neognath birds as proxies where osteological correlates were not clear (see Bite force for further information; Rayfield, 2007; Cuff et al., 2015). We did, however, produce a second Struthio model with simulated palatobasal (parasphenoid–pterygoid) and otic (quadrate-squamosal) joints (Bailleul et al., 2017). It should be made clear that this does not model the entire extent of rhynchokinesis observed in Struthio, which would take more than adding just these two pairs of joints (and is also beyond the scope of the study). The inclusion of these joints, however, does allow some insight to be gained into their functional role during feeding behaviors. Results from the "jointed" Struthio model can be found in the Supplementary Information. Ornithomimus was chosen due to its frequently noted high degree of morphological convergence with Struthio and the availability of complete and threedimensionally preserved cranial material (Cuff & Rayfield, 2015). Alligator was included as an extant representative of the pseudosuchian lineage and as an outgroup with markedly different cranial morphology from the other study taxa due to the presence of teeth and a dorso-ventrally flattened and mediolaterally broader skull (Busbey, 1989). This sample enables a more thorough investigation into whether morphological convergence leads to functional convergence among unrelated taxa with ostrich-like bauplans.

2.2 | Retrodeformation and digital reconstruction

The CT image files of Effigia were imported into Avizo (version 7.0 & 8.0, Visualisation Science Group) for segmentation from the surrounding matrix. The individual skull elements were highlighted and separately labeled using the segmentation editor in Avizo to produce surface models and volumes. In some cases, individual skull bones had broken into multiple pieces during fossilization and post-fossilization processes (compaction, uplift, etc.; Figure S1). All elements were subsequently retrodeformed to their hypothesized original morphology and realigned to restore the skull to an approximate nondeformed condition (Figure S1). Retrodeformation was carried out in Avizo. Only two Effigia skulls are known, one largely complete and one partially preserved, and both exhibit some deformation in the form of breakage, displacement, plastic deformation, or a combination of some or all three (Nesbitt, 2007; Nesbitt & Norell, 2006). The restoration process followed the steps outlined by Lautenschlager (2016) and was informed by: the topographic relationships of individual elements in the 3D CT scan data; identification and subsequent repair of cracks and holes; and osteological comparisons with closely

related taxa, such as extant crocodylians. Osteological features that were badly damaged or missing entirely on one side of the skull were substituted by mirroring the corresponding feature from the opposite side of the skull, assuming bilateral symmetry. Palatal features were assembled first, followed by the remainder of the cranium, and lastly the mandibles, in order to better identify the original dimensions of the skull, in particular reconstruction of the cranial and mandibular widths through the quadrate-squamosal and quadrate-articular articulations and through the contact point of the ectopterygoidmandible, lacrimal and jugal (Figure S1). It should be noted that the palate morphology of Effigia is unique, so the reconstruction was based on the constraints of other skull bones and with broad comparisons with other archosaurs such as crocodylians. Annotated diagrams of the complete retrodeformed cranium and mandible are shown in Figure 1.

The full Ornithomimus retrodeformation protocol can be found in Cuff and Rayfield (2015) but the main steps are noted here for completeness. Retrodeformation took place in Avizo 7.0. All Ornithomimus cranial material exhibits some form of deformation, thus specimens ROM 841 and ROM 851 were observed first hand to inform the process. Where relevant, the cranial morphology of other ornithomimids such as Sinornithomimus dongi (Kobayashi & Lü, 2003) and Gallimimus bullatus (Osmólska et al., 1972) were used to aid the process. The palatines and pterygoids exhibited quite large degrees of mediolateral displacement and overlap. The palatal bones were therefore individually segmented and aligned and then used as a marker for estimating the mediolateral dimensions for the rest of the cranium. Subsequent filling of cracks, holes and missing material were performed as per Lautenschlager et al. (2013).

To increase the degree of model realism, keratinous rhamphothecae were added to the crania and mandibles of the three edentulous study taxa using Avizo. All rhamphothecae were modeled around 3 mm thick, informed by tentative soft tissue preservation in ornithomimids (Cuff & Rayfield, 2015; Norell et al., 2001), and modeled as a homogenous and isotropic layer that attached directly to the bone. Although this does not capture the full biological complexity of rhamphothecae, it does enable more representative comparisons between the study taxa. The modeled Struthio rhamphotheca covers much of the premaxilla and maxilla on the cranium, partially surrounding the nares, and extends to the jugal bar along the upper jaw. Accurately inferring the presence and shape of rhamphothecae in extinct taxa is difficult as these non-mineralized tissues are rarely preserved (Norell et al., 2001), and there are no conclusive osteological correlates for these structures

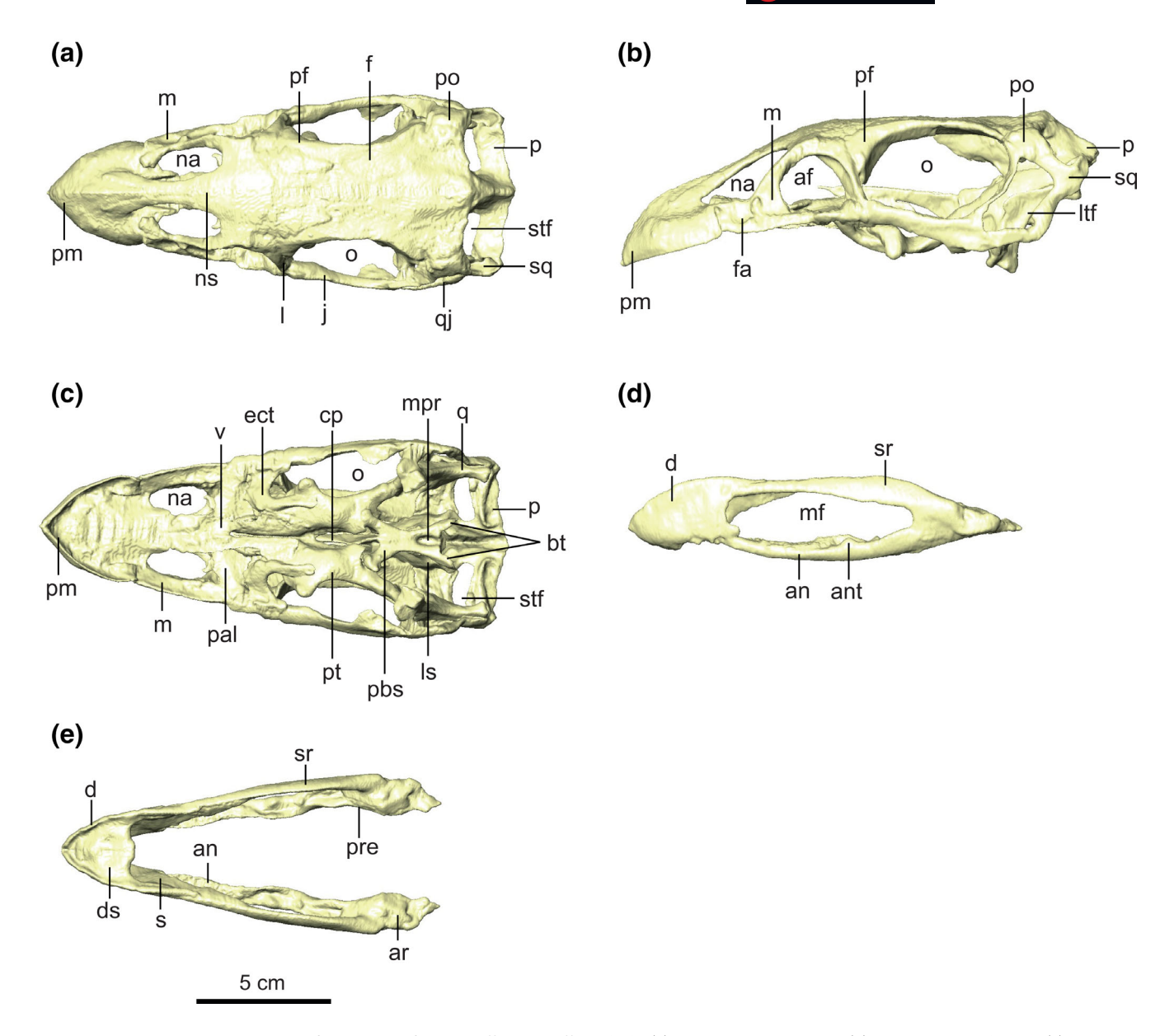


FIGURE 1 Labeled diagrams of the retrodeformed *Effigia okeeffeae* skull, (a) cranium lateral view, (b) cranium dorsal view, (c) cranium palatal view, (d) mandible lateral view, (e) mandible dorsal view. Abbreviations: af, antorbital fenestra; an, angular; ant, angular tuber; ar, articular; bt, basal tuber; cp; cultiform process; d, dentary; ds, dentary shelf; ect, ectopterygoid; f, frontal; fa, foramen; j, jugal; l, lacrimal; ls, laterosphenoid; ltf, lateral temporal fenestra; m, maxilla; mf, mandibular fenestra; mpr; median pharyngeal recess; na, naris; ns, nasal; o, orbit; p, parietal; pal, palatine; pbs, parabasisphenoid; pf, prefrontal; pm, premaxilla; po, postorbital; pre, prearticular; pt, pterygoid; q, quadrate; qj, quadratojugal; s, splenial; sq, squamosal; sr, surangular; stf, supratemporal fenestra; v, vomer. All models to scale

(see Lautenschlager et al., 2014 and Cuff & Rayfield, 2015 for a discussion). Two different rhamphotheca morphologies, dubbed "small beak" and "large beak," were therefore created for both *Effigia* and *Ornithomimus* to encompass the lower and higher ranges of possible shapes based on the shapes of the cranial bones (Figure 2). The small beak cranial rhamphotheca of *Effigia* covers the anterior half of the premaxilla (Figure 2a,b) and the small beak rhamphotheca of *Ornithomimus* covers the ventro-lateral and ventral

margins of the premaxilla and anterior half of the maxilla (Figure 2i,j). The large beak cranial rhamphotheca of *Effigia* extends to the anterior edges of the nasal and maxilla bones (Figure 2c,d), and the large beak rhamphotheca of *Ornithomimus* extends to the anterior margins of the antorbital fenestrae without covering the nares (Figure 2k,l). The small beak mandibular rhamphotheca of *Effigia* covers the anterior half of the dentary (Figure 2e,f) and the large beak mandibular rhamphotheca extends to the posterior margin of the dentary (Figure 2g,h).

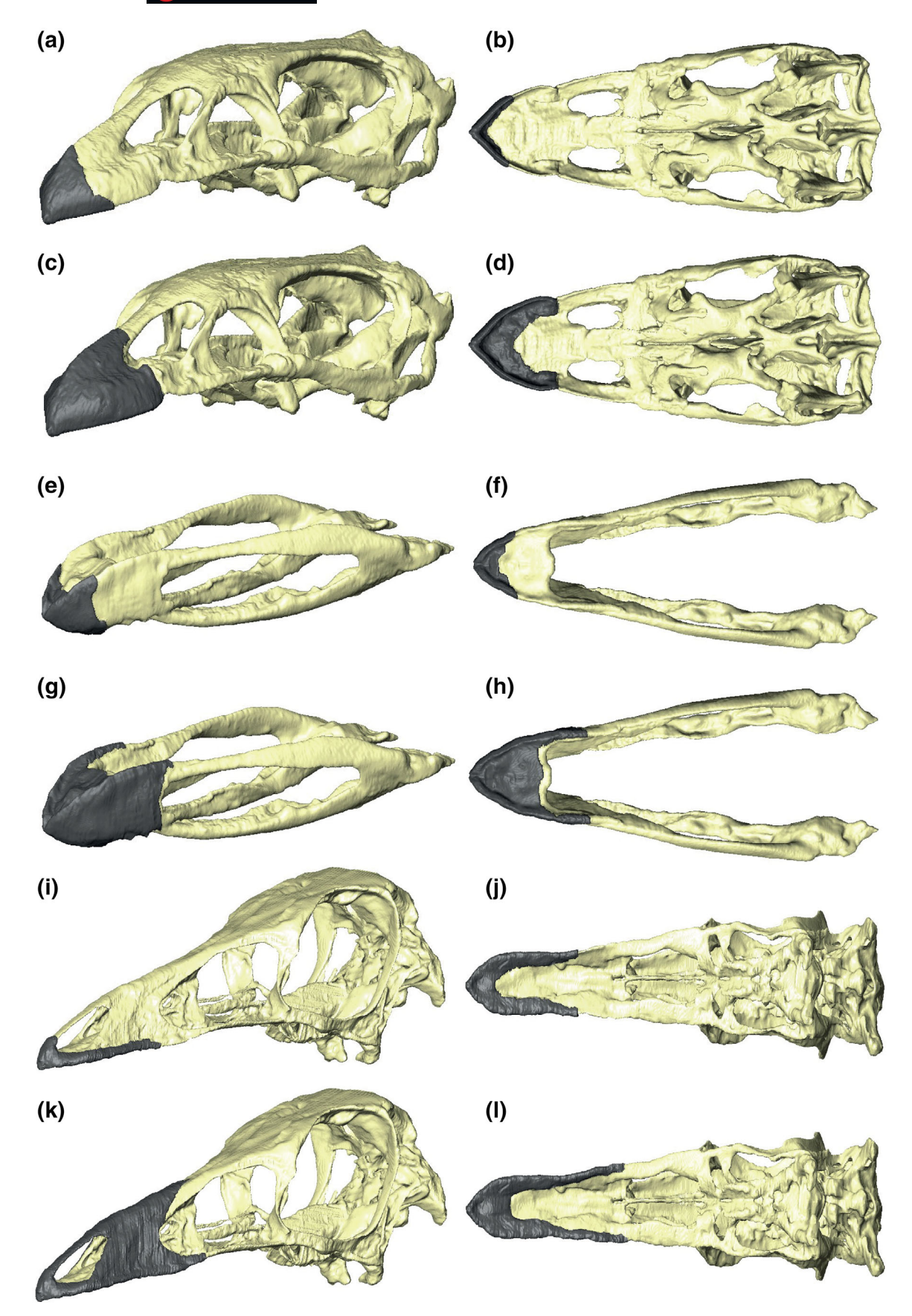


FIGURE 2 Legend on next page.

2.3 | Muscle reconstructions

Muscle origination and insertion sites for *Effigia* (Figure 3) were identified for each jaw adductor muscle independently based on osteological correlates such as muscle scars, ridges and depressions. Where such features were badly preserved, obscured or altogether absent, extant phylogenetic bracketing was used to infer the positions and extents of muscle attachment sites. Following Holliday and Witmer (2007), *Effigia* myoanatomy was bracketed between that of extant crocodylians (Busbey, 1989; Holliday et al., 2013) and birds (Lautenschlager et al., 2014; Webb, 1957), with the extant lepidosaur *Sphenodon punctatus* (Holliday & Witmer, 2007; Jones et al., 2009) used as an outgroup. Reconstructions of the myoanatomy of non-avian theropod dinosaurs (Holliday, 2009; Lautenschlager, 2013) were also consulted as independent reference points.

The origin and insertion sites for each muscle were connected by thin cylinders connecting the centre of each site. Where necessary, cylinder pathways were adjusted to avoid cross-cutting each other and osteological structures (Curtis et al., 2009). Additional cylinders were then plotted from the edges of each muscle attachment site to produce simplistic frames that were "fleshed out" to create full 3D muscle reconstructions. The final size and shape of each muscle was determined by the geometry of the surrounding bone surfaces and by preventing any cross-cutting between muscles.

Based on phylogenetic bracketing, we infer that Effigia had a fibrocartilaginous sesamoid, similar (though not necessarily homologous) to the cartilago transiliens of extant crocodylians, within its adductor chamber (Tsai & Holliday, 2011). In extant crocodylians, this structure develops as a fibrous nodule within the medial portion of the m. pseudotemporalis superficilias tendon, becoming continuous with the m. intramandibularis and eventually forming connections with immediately surrounding muscles and a fibrous connection to the coronoid eminence (Tsai & Holliday, 2011). The sesamoid serves to prevent damage and tendon flattening as associated muscles wrap around a trochlear surface; in the case of crocodylians this relates to the m. pseudotemporalis and m. intramandibularis complex passing over the pterygoid wing, although analogous structures are found in turtles within the adductor mandibulae externus group

where it passes over the trochlear process of the quadrate (Bramble, 1974), in a range of squamates where it is associated with the quadrate (Montero et al., 2017), and in birds where sesamoids are commonly found within the jugomandibular ligament (Burton, 1973).

A fibrocartilaginous linkage between the m. pseudotemporalis superficialis and the m. intramandibularis was noted in birds and turtles by Holliday and Witmer (2007), leading Tsai and Holliday (2011) to suggest the possibility of homology between these structures; if this were the case a fibrocartilaginous link between these muscles would be plesiomorphic for archosaurs.

In Effigia the path of the m. pseudotemporalis superficialis and m. intramandibularis wraps around the pterygoid wing and at the same point is laterally constricted by the surangular. The pterygoid wing itself is dorsolaterally broad and rounded rather than thin and flat. therefore providing a smooth trochlear-like surface for a hypothetical intertendon to articulate around. Due to the similarity in position to the fibrocartilaginous linkage in turtles and birds (Holliday & Witmer, 2007), the presence of cranial sesamoids at tendinous pressure-points in a range of phylogenetically bracketing taxa and the likely application of regular pressure at this point, we reconstructed a small sesamoid at this point in Effigia. The sesamoid was considered in our muscle reconstructions and in placing the muscle forces for the FEA models. Due to the difficulty in modeling fibrocartilaginous structures suspended between muscle bodies, the sesamoid was not incorporated as a separate component in the FEA models. However, the effect of this sesamoid on muscle vectors was retained during analyses as the mandible and cranium are modeled separately.

2.4 | Bite force

Muscle force estimates $(F_{\rm mus})$ were calculated using a modified version of the dry skull method of Thomason (1991). Average cross-sectional areas (CSA) of each muscle were obtained using the Avizo material statistics module, which lists the respective CSA values for each individual material (in this instance the muscles).

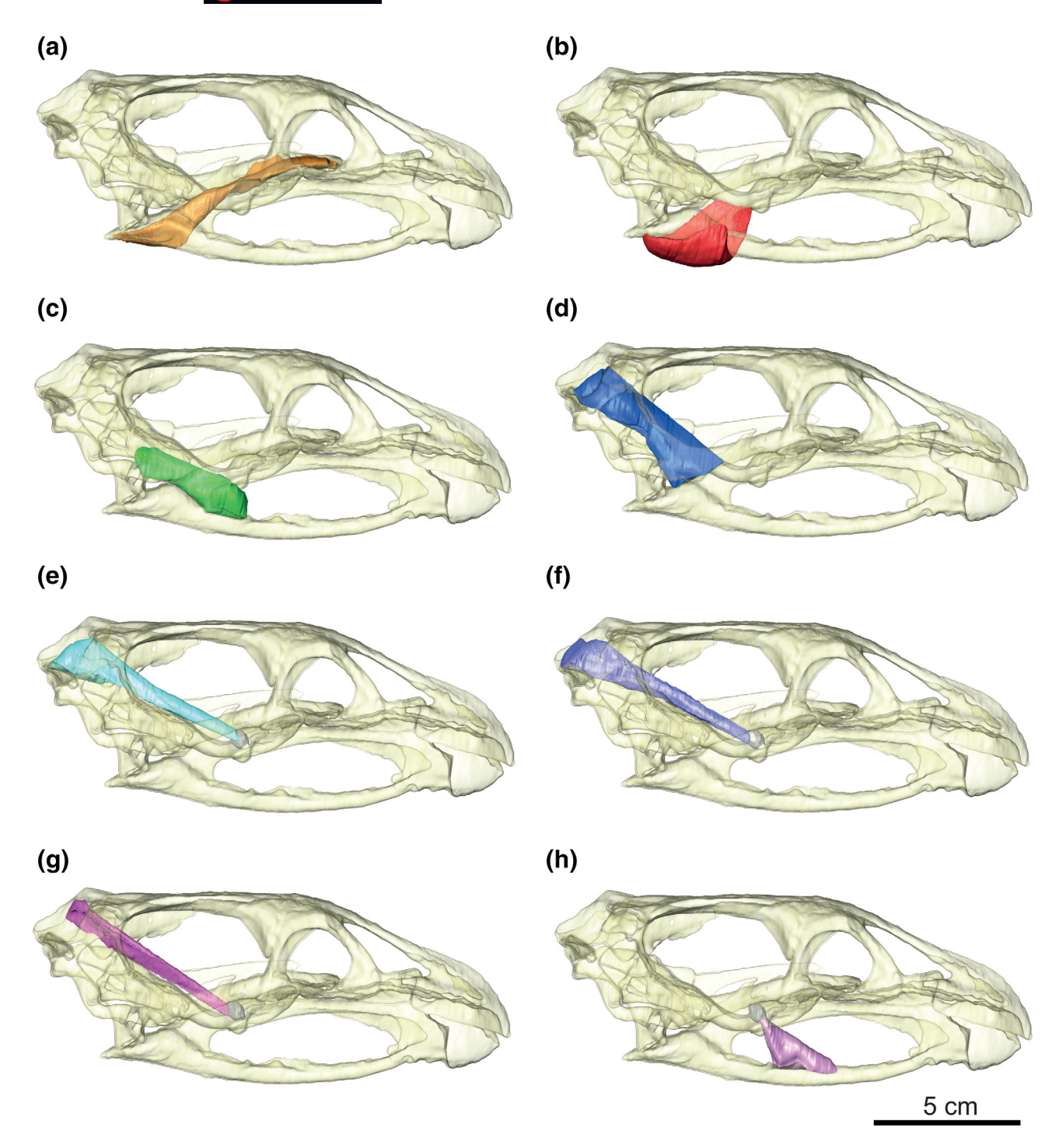


FIGURE 3 Reconstructed adductor musculature of *Effigia okeeffeae* shown in right lateral view. (a) m. pterygoideus dorsalis, (b) m. pterygoideus ventralis, (c) m. adductor mandibulae posterior, (d) m. adductor mandibulae externus superficialis, (e) m. adductor mandibulae externus medialis, (f) m. adductor mandibulae externus profundus, (g) m. pseudotemporalis superficialis, (h) m. intramandibularis. The mandibular insertions of the muscles in parts (e-h) are reconstructed as attaching to a cartilaginous sesamoid, the cartilago transiliens. The sesamoid was included in the muscle reconstructions but excluded from finite element analyses due to the unknown material properties of cartilaginous structures

Muscle force was calculated for each muscle individually (i.e., for one side of the skull), using Equation (1), assuming an isometric muscle stress value (σ) of 0.3 N mm⁻², following Thomason (1991) and Lautenschlager et al. (2013):

$$F_{\text{mus}} = \text{CSA} \times \sigma$$

This method is rather simplistic as it does not account for the pennation angle of the individual muscle fibers, likely resulting in underestimations of muscle and bite forces. Muscle forces acting in dorsoventral directions were used for bite force lever mechanics as anteroposterior and mediolateral muscle forces have a very limited influence on jaw closure (Cuff & Rayfield, 2015). Muscle insertion angles from the vertical axis were measured directly in the three-dimensional model in both the sagittal (α) and the coronal planes (β) using the Avizo measurement tool. The resulting muscle force that accounts for insertion angle $(F_{\rm res})$ was calculated using Equation (2):

$$F_{\rm res} = F_{\rm mus} \times \cos\alpha \times \cos\beta$$

Final bite force estimates (F_{bite}) were calculated independently for each muscle using Equation (3):

$$F_{\text{bite}} = (F_{\text{res}} \times L_{\text{inlever}}) / L_{\text{outlever}}$$

 $L_{
m outlever}$ denotes the distance between the bite point to the jaw joint and $L_{
m inlever}$ denotes the distance between the insertion point of the respective muscle and the jaw joint. All distances were measured in horizontal view in Avizo. The calculated values for these parameters can be found in Table S1.

Muscle forces for Alligator and Ornithomimus were derived from Montefeltro et al. (2020) and Cuff and Rayfield (2015) respectively. It should be noted that the Ornithomimus muscle forces are rather conservative estimates and the actual forces in life might have been slightly greater (Cuff & Rayfield, 2015). Estimated jaw muscle forces for Struthio have never been published, so these forces were estimated by identifying origin and sites based on osteological (Webb, 1957). Where correlates were not clear, the myoanatomy of the extant common buzzard, Buteo buteo (Lautenschlager et al., 2014), and rock dove, Columba livia (Jones et al., 2019), were consulted. Despite the long independent evolutionary histories of Struthio and neognath birds, avian adductor muscle morphology is relatively conserved (Holliday & Witmer, 2007), allowing neognath muscles to be used as proxies where necessary. The CSA of each muscle was measured in ImageJ (National Institutes of Health), multiplied by the isometric stress value to attain the muscle force.

2.5 | Finite element analysis

The 3D models of all specimens were imported into Hypermesh 11 (Altair Engineering) for the generation of solid tetrahedral meshes (consisting of approximately 300,000 elements per model). All cranial models were scaled to the same surface area as the *Effigia* cranium to

enable more representative comparisons between archosaurs (Dumont et al., 2009). The muscle forces of the other archosaurs were also scaled accordingly. Scaling information can be found in Table 1. All models were loaded with maximum adductor muscle forces as calculated in Table 2. Loads were applied across multiple nodes at the inferred muscle origination and insertion sites of the crania and mandibles, respectively. This was performed using a custom-built macro (Altair UK) which simultaneously loads multiple nodes projected towards a node(s), resulting in a vector equivalent to the line of action of each muscle.

To further enable realistic comparisons between these archosaur taxa, specimens were assigned the same material properties for bone based on values for Alligator mandibular bone (E = 15.0 GPa, v = 0.29; Zapata et al., 2010). Material properties for teeth were also based on values for Alligator (E = 60.4 GPa, v = 0.31; Zapata et al., 2010). Mateproperties for the keratinous rhamphothecae (E = 1.04 GPa, v = 0.4) were based on extant bird beaks and taken from Chen et al. (2008). Material properties for the areas of bone that immediately surround the palatobasal and otic joints in the jointed Struthio model were based on Alligator connective tissue (E = 0.09 GPa, v = 0.3; Porro et al., 2013). All material properties within the models were treated as isotropic and homogeneous. The skull models were constrained from rigid body motion in all degrees of freedom at the parietals and the condyles of the mandibular capitulum of the quadrates. For all models and feeding simulations four nodes were constrained at the parietals and four nodes were constrained on each of the quadrates (12 in total). Usually, the occipital condyle and paroccipital process are used as the positions for these constraints (e.g., Lautenschlager et al., 2013), but the posterior braincase of Effigia was not scanned and is therefore unavailable. For the Effigia mandible, four nodes were constrained in all degrees of freedom at the articulation point on the dorsal surface of the articular (eight in total).

All models were imported into Abaqus (Version 6.10; Simulia) for analysis and postprocessing. The following feeding-related simulations were performed for each model:

(a) Anterior bite. Bilateral biting at the tip of the snout in the premaxilla. One node was constrained on each of the left and right side of the jaws (two in total) in all degrees of freedom. For all cranial models except *Alligator*, the constraints were placed on the rhamphotheca covering the anteroventral tip of the premaxillae. For both *Effigia* mandible models, the constraints were placed on the rhamphotheca covering the dorsoanterior tip of the dentaries. For *Alligator*, the constraints were placed on the anterior-most tooth on each side of the premaxilla.

TABLE 1 Scaling information for the model crania of the study archosaurs

	Effigia	Ornithomimus	Struthio	Alligator
Actual cranium length (mm)	166.6	185	200.3	371
Initial model surface area (mm²)	43,113	52,085	72,348	396,765
Surface area and muscle force scale factor	_	1.208	1.6781	9.202
Length scale factor	_	1.099	1.295	3.033
Scaled model cranium length (mm)	_	168.314	154.622	122.296

Note: Ornithomimus, Struthio and Alligator model crania were scaled down to the same surface area as the Effigia cranium.

	Muscle for	Muscle force (N)					
Muscle	Effigia	Ornithomimus	Struthio	Alligator			
m. PTd	10.2	14.2/17.1	20.5/34.3	15.8/145.8			
m. PTv	60.6	5.9/7.1	46.6/78	19/174.5			
m. AMP	15.2	12.4/15	5.2/8.8	8.9/81.7			
m. AMEM	14	7.2/8.7	30.3*/50.7*	4.9/45.3			
m. AMEP	12.6	10.7/12.9	8/13.4	4.4/40.1			
m. AMES	22.5	8.7/10.5	—/—	10.1/92.8			
m. PSTs	12.2	8.6/10.4	1.78/2.9	3.5/32			
m. PSTp	_	_	1.8/3.1	2.8/25.7			
m. IRA	21.7	_	_	_			
Sum	168.9	67.6/81.7	114.3/191.2	69.3/637.8			

TABLE 2 Muscle force estimates of individual jaw adductor muscles for study archosaurs

Note: Muscle force estimates are unilateral. See Table S1 for more information on how Effigia muscle forces were measured and calculated. Ornithomimus, Struthio and Alligator force estimates are presented as scaled values (forces used in finite element analyses where the crania are scaled to the same surface area as the Effigia cranium) and unscaled values (forces from actual crania size), respectively. See Table S1 for more detailed information on how scaled muscle forces were calculated. Effigia and Struthio force estimates were calculated in this study. Struthio m. AMEM force estimates denote the derived m. AMEM/S muscle group found in extant birds (Holliday & Witmer, 2007). Unscaled Ornithomimus estimates are from Cuff and Rayfield (2015) and unscaled Alligator estimates are from Montefeltro et al. (2020). The m. PSTp was not calculated for Effigia and Ornithomimus (see Effigia musculature in the Results section for more information) and the m. IRA was not calculated for Ornithomimus, Struthio and Alligator. All values to 1 d.p.

- (b) Middle bite. Bilateral biting at the middle of the snout. One node was constrained on each of the left and right side of the jaws (two in total) in all degrees of freedom. For the small-beaked Effigia models, the constraints were placed on the posterior-most edge of the premaxilla and dentary in the cranium and mandible, respectively. For the small-beaked Ornithomimus, the constraints were placed on the maxilla. For the large-beaked cranial models of Effigia and Ornithomimus and for Struthio, the constraints were placed on the rhamphothecae that covers the maxillae. For the large-beaked Effigia mandible model, the constraints were placed on the rhamphotheca that covers the posterior edge of the dentary. For Alligator, the constraints were placed on the fourth tooth in the maxillary tooth row as these are the main teeth used for seizing prey (Erickson et al., 2012).
- (c) Posterior bite. Bilateral biting at the inferred posterior functional end of the snout. One node was constrained on each of the left and right side of the jaws (two in total) in all degrees of freedom. For both beak models of *Effigia*, the constraints were placed on the maxilla and surangular of the crania and mandibles, respectively. For *Struthio*, the constraints were placed on the rhamphotheca that covers the posterior region of the maxillae. For both beak models of *Ornithomimus* the constraints were placed on the jugals. For *Alligator*, the constraints were placed on the posterior-most tooth in the maxilla and dentary.
- (d) Pecking. An external force moving dorsoposteriorly towards the cranium was used to simulate a feeding-related pecking action at the inferred functional tip of the snout. We applied a force of 340 N to one node

at the snout tip. The adductor muscles generate this magnitude (Table 2) after accounting for both halves of the cranium. As the cranium can withstand this force, we applied it to the rostrum. For both beak morphologies of *Effigia* and *Ornithomimus* and for *Struthio*, the external force contacts the anterior tip of the rhamphotheca. For *Alligator*, the external force contacts the anterior tip of the premaxilla.

Von Mises stress (a measure of overall structure strength under loading conditions) were displayed as contour plots for all simulations to enable visual assessments of the relative performance of the crania and mandibles. Stresses were also measured at 10 equally spaced locations along the dorsal and palatal surfaces of each cranium to provide more detailed assessments on model performance. The highly derived condition of the bones in the Struthio cranium (Cuff et al., 2015) hinders identification of homologous landmarks between pseudosuchian and avemetatarsalian skulls. Therefore, the dorsal and palatal surfaces of each cranium was divided into 10 sections of equal length along a longitudinal axis with von Mises stresses measured in the approximate centre of each section. For Alligator, many of the sampling locations along the palatal surface are from the secondary, or closed, palate, which is a bony plate comprising the maxillae, palatines and pterygoids that separates the nasal and oral passages (Busbey, 1995; Rayfield & Milner, 2008). This structure is unique to Alligator among our study taxa. Measurement locations across the dorsal and palatal surfaces of all crania are shown in Figure S2. Measurement locations are the same in the jointed and non-jointed Struthio models.

3 | RESULTS

3.1 | Retrodeformation redescriptions

Retrodeformation enabled new anatomical information to be gained on the overall morphology of the skull as well as on specific cranial elements. Some of the main results are highlighted here and further detailed descriptions can be found in the Supplementary Information. As a disclaimer, accurate anatomical interpretations of Coelophysis Quarry material can be problematic due to the difficulty in identifying whether material has been subjected to taphonomic processes and the extent to which these processes have occurred. Notably, plastic deformation has been observed in Coelophysis Quarry material, such as specimens of the theropod dinosaur Coelophysis bauri (Colbert, 1989; Schwartz & Gilette, 1994). Our interpretations and redescriptions of the retrodeformed Effigia material are therefore cautious and based on the available osteological evidence as preserved.

With respect to general skull morphology, the skull table is reconstructed as generally flat in lateral view, in contrast to the dorsally bowed outline shown in Nesbitt and Norell (2006) and in Shuvosaurus inexpectatus due to the lack of dorsal curvature of the frontals in the new reconstruction (Figure 1). The ventral border of the cranium, comprising the premaxillae, maxillae and jugals, is inferred here to be anteroposteriorly concave in lateral view (Figure 1) rather than straight as described previously (Nesbitt, 2007; Nesbitt & Norell, 2006). Consequently, the craniomandibular joint is now deflected ventrally with respect to the rest of the skull (Figure 1). Our new reconstruction results in mandibles that are reconstructed as dorsoventrally taller in lateral view than those presented by Nesbitt (2007) due to the greater curvature of the angular (Figure 1). The dorsal surface of the dentaries exhibited strong anteroventral curvature towards their anterior extremities following segmentation, contrasting with the flat dorsal surface that was previously reconstructed (Nesbitt & Norell, 2006). As a result, the dentaries now have a more precise contact and greater overlap with the ventral shelves of the premaxillae during full jaw closure (Figure 1).

With regard to specific elements, a postero-laterally projecting prong from the main body of the nasal bone fits within, and partially overlies a complementary groove on the dorsal margin of the lacrimal. The articulation of the lacrimal with the jugal differs from the reconstruction of Nesbitt and Norell (2006); the distal end of the lacrimal ventral process does not appear to expand anteroposteriorly along the dorsal surface of the jugal. Instead, the lacrimal tapers towards its ventral extremity, ending in a rounded tip that inserts into a sulcus on the dorsal surface of the jugal. The ventral process of the prefrontal, which was not described by Nesbitt (2007), abuts the lacrimal obliquely and tapers ventrally. Lastly, upon segmentation of the pterygoids, a pair of deep sockets were identified medially to the quadrate ala, which form recesses for the reception of the basipterygoid processes.

3.2 | Effigia musculature

3.2.1 | m. pterygoideus dorsalis

The m. pterygoideus dorsalis (m. PTd) most likely originates from a deep fossa on the dorsal surface of the palatines, directly posterior to the pila postchoanalis (Figure 3a). The dorsal extent of the m. PTd is bounded by a secondary palatine plate, dorsal to the main element, extending laterally from the palatine's medial expansion. This is inferred largely from the generally plesiomorphic muscle position in extant crocodylians, birds and lepidosaurs

(Busbey, 1989; Holliday et al., 2013; Holliday & Witmer, 2007; Lautenschlager et al., 2014) and from reconstructions in dinosaurs (Holliday, 2009; Lautenschlager, 2013). Medially, the m. PTd is bordered by the dorsal vaulting at the sagittal contact of the pterygoids and laterally by their dorsally expanded wing. As in extant archosaurs, the m. PTd passes over the posterior edge of the lateral process of the pterygoid and plunges posteroventrally towards its mandibular insertion (Figure 3a).

The mandibular insertion is clearly defined as a flat ventromedial surface of the surangular and articular, ventral to the quadrate articulation (Figure 3a). The dorsal extent of the attachment is defined by a medially-projecting crest at the junction of the surangular and prearticular, and posteriorly it extends to the posterior limit of the short retroarticular process. The anterior extent of the attachment is poorly defined.

3.2.2 | m. pterygoideus ventralis

The origin of the m. pterygoideus ventralis (m. PTv) is poorly defined. The condition in *Effigia* is therefore inferred from the condition in crocodylians and birds; attachment along the posteroventral edge of the pterygoid flange. As with the m. PTd, the m. PTv is directed ventrally and posteriorly before wrapping ventrally around the mandible, directly ventral to the quadrate-articular articulation (Figure 3b).

The insertion of the m. PTv is marked by a fossa on the ventrolateral surface of the mandible (Figure 3b). This inference is supported by extant phylogenetic bracketing as the muscle attaches to this area in crocodylians and palaeognaths (Holliday, 2009). The reconstructed size of the m. PTv is based on that from a juvenile *Alligator* (Holliday et al., 2013) due to a lack of constraining osteological evidence.

3.2.3 | m. adductor mandibulae posterior

The m. adductor mandibulae posterior (m. AMP) is one of the most phylogenetically conserved muscles within the adductor chamber, maintaining generally consistent origination and insertion points throughout Sauropsida (Holliday & Witmer, 2007). The m. AMP originates from the lateral surface of the quadrate in Sphenodon and Struthio (Holliday & Witmer, 2007; Jones et al., 2009); and has been reconstructed in a similar position in the therizinosaurian dinosaur Erlikosaurus andrewsi (Lautenschlager, 2013), a range of ornithomimosaurian dinosaurs (Cuff & Rayfield, 2015) and sauropod dinosaurs (Button et al., 2016; Young et al., 2012). Extant crocodylians display a derived condition, with the m. AMP originating from the ventral surface of the quadrate; as the quadrate of *Effigia* is far more similar to those of birds, dinosaurs and *Sphenodon*, an origination for the m. AMP based on extant crocodylians is excluded. The insertion of the m. AMP is within the internal mandibular fossa (Holliday, 2009), a condition shared in all taxa noted above. *Effigia* displays a clear fossa on the lateral surface of the quadrate, constraining the muscle posteriorly and laterally (Figure 3c). This muscle is inferred to extend anteriorly into a groove that excavates the dorsomedial surfaces of the angular and prearticular, at the anterior end of which the muscle terminates (Figure 3c).

3.2.4 | m. adductor mandibulae externus superficialis

The origin of the m. adductor mandibulae externus superficialis (m. AMES) is based on a combination of the muscle and bone morphology in crocodylians and ancestral lepidosaurs, and the large dorsal temporal fenestra of Effigia. In crocodylians, the origin is on the ventrolateral surface of the quadrate whereas the origination in ancestral lepidosaurs is the medial surface of the supratemporal bar (Holliday et al., 2013; Holliday & Witmer, 2007). The origin of the m. AMES in crocodylians is defined by a groove created by a flange of the quadrate following its curve posterodorsally until it nears the mandibular articulation (Holliday et al., 2013). In Effigia, the quadrate, by contrast, curves posterodorsally but displays a similar flange and groove to that seen in crocodylians (Figure 3d) (Nesbitt, 2007). This flange forms a dorsally/anterodorsally orientated channel that is directed posterodorsally towards the lateral border of the supratemporal fenestra. The m. AMES of Effigia is therefore suggested to have originated from the lateral border of the supratemporal fenestra and formed additional attachments to the lateral quadrate as it followed this channel towards its mandibular insertion (Figure 3d).

The insertion includes the flattened dorsal surface of the posterior surangular, immediately anterior to the quadrate articulation (Figure 3d). This is consistent in the majority of phylogenetic bracketing taxa. The primary medial constraint of the m. AMES is the quadrate, although it is also bordered medially by the m. adductor mandibulae externus medialis. Laterally, the m. AMES is bordered by the squamosal, postorbital, quadratojugal and jugal (Figure 3d).

3.2.5 | m. adductor mandibulae externus medialis

The m. adductor mandibulae externus medialis (m. AMEM) likely attached to the posterior margin of the supratemporal fenestra (Figure 3e). Although no distinct

demarcations of where this muscle attached are preserved in *Effigia*, its fenestral morphology closely resembles those of non-avian dinosaurs and lepidosaurs, whose m. AMEM originate from a similar area (Holliday, 2009; Holliday & Witmer, 2007; Lautenschlager, 2013), in contrast to the condition in crocodylians, where the m. AMEM originates from the trapezoidal region of the quadrate (Busbey, 1989).

The mandibular insertion of the m. AMEM is based largely on that of extant crocodylians. Due to the dorsoventrally flattened morphology of crocodylian skulls, their temporal muscles must project further laterally than in birds and dinosaurs in order to reach their mandibular insertion points. The muscles must therefore wrap around the pterygoid wing. As these muscles wrap around the pterygoid, they link to the m. intramandibularis (m. IRA) via the cartilago transiliens. At this location, these muscles terminate and are secondarily inserted onto the mandible via the m. IRA. The *Effigia* skull is not dorsoventrally flattened, but the anteriorly shifted jaw articulation in *Effigia* forces the temporal muscles to extend further anteriorly to attach to the mandible (Figure 3e). The temporal muscles must therefore wrap around the pterygoid wing (Figure 3e).

3.2.6 | m. adductor mandibulae externus profundus

The m. adductor mandibulae externus profundus (m. AMEP) originates from the lateral margin of the supratemporal fenestra (Figure 3f), similar to lepidosaurs and dinosaurs (Holliday et al., 2013; Holliday & Witmer, 2007; Lautenschlager et al., 2014).

The extent of the m. AMEP mandibular insertions are similar to those of the m. AMEM and it is inferred to have inserted into the cartilago transiliens as in crocodylians. However, as mentioned above, the sesamoid was not included in our FEA models. The m. AMEP is constrained laterally by the m. AMEM and medially by the m. pseudotemporalis superficialis (m. PSTs) (Figure 3f). As these constraints would have been made entirely of soft tissue and are hypothesized, the muscle group consisting of the m. AMEM, m. AMEP and m. PSTs was reconstructed with a generally cylindrical cross-section, bulging only to the extent allowed by other better constrained myological and osteological features (Figure 3f).

3.2.7 | m. pseudotemporalis superficialis

The m. pseudotemporalis superficialis most likely attached to the medial surface of the supratemporal fenestra (Figure 3g). This is inferred from the high degree of similarity in temporal morphology between *Effigia*, lepidosaurs and dinosaurs (Holliday, 2009; Holliday & Witmer, 2007).

The mandibular attachment is similar to those of the m. AMEM and m. AMEP but, as previously explained, the insertion site is the cartilago transiliens and the m. IRA (Figure 3g).

3.2.8 | m. pseudotemporalis profundus

The m. pseudotemporalis profundus (m. PSTp) has not been reconstructed in Effigia for two reasons: (a) an ossified epipterygoid—a clear origin site in lepidosaurs and many dinosaurs (Holliday, 2009)—is not preserved in Effigia and appears to have been absent; and (b) Effigia does not display any osteological correlates for the origin of the m. PSTp. The presence of this muscle is debated in crocodylians and, if present, is likely to be a vestigial structure consisting of a short, thin muscle originating from the lateral bridge of the laterosphenoid and merging into the dorsal surface of the m. PTd (Holliday et al., 2013). If the crocodylian condition was present in Effigia, the muscle would contribute very little to bite force. The m. PSTp is also not reconstructed in the comparative ornithomimid cranial FE models (Cuff et al., 2015). Without osteological correlates, reconstructing the m. PSTp could compromise the FE model validity.

3.2.9 | m. intramandibularis

The m. intramandibularis is interpreted to extend from the anteroventral surface of the hypothesized cartilago transiliens to the dorsomedial surface of the angular and prearticular (Figure 3h). The mandibular insertion is marked by an anteroposterior groove at the contact between these two mandibular elements. This is a rather conservative interpretation because we cannot rule out the possibility that the m. IRA extends more anteriorly, as exhibited by extant crocodilians, filling more of the intramandibular space and attaching to the dentary and splenial (Bona & Desojo, 2011; Holliday et al., 2013). Such a condition has been reconstructed for non-avian dinosaurs (e.g., Gignac & Erickson, 2017). Posteriorly, the m. IRA is constrained by the anterior margin of the m. AMP as the latter muscle also inserts into this groove. Dorsolaterally, the m. IRA is constrained by the surangular (Figure 3h).

3.3 | Finite element analysis results

3.3.1 | Muscle force estimates

Our jaw muscle reconstructions demonstrate that *Effigia* has the largest total jaw-closing muscle force among the

scaled archosaur models, and exhibits double the total force of the unscaled *Ornithomimus* (Table 2). The reconstruction of the m. IRA in *Effigia* but not in the other study archosaurs somewhat limits discussion of the relative muscle contributions between archosaur taxa. Nevertheless, some informative comparisons can be made. For example, in *Effigia* the m. PTv provides the largest contribution to total muscle force, as in *Struthio* and *Alligator*, and has the largest force among the m. PTvs of the scaled archosaurs (Table 2). In contrast, the *Effigia* m. PTd produced the lowest force of those among the scaled archosaurs (Table 2). Overall, the *Effigia* adductor mandibulae forces are most similar to those of *Ornithomimus* (Table 2) among the taxa examined.

3.3.2 | Feeding simulations

To facilitate comparisons between the archosaurs considered herein, von Mises stress distributions across crania and mandibles are presented for each feeding simulation (Figures 4–7) and stress values at specific measurement locations across the dorsal and palatal cranial surfaces (Figures 8 and 9, respectively) are presented with reference to taxon and rhamphotheca morphology. Results from the jointed *Struthio* model are broadly similar to those of the un-jointed model, with the exception of localized patterns around the palatobasal and otic joints (see Supporting Information and Figure S3).

During anterior bite simulations, the Effigia smallbeaked cranium model displays high stress around the following areas: the anterior surfaces of the squamosals; the ventral and posterior surfaces of the quadrates; the ventral and lateral surfaces of the pterygoids; the contact between the premaxilla and nasal (hereafter referred to as the nasal bridge) and the posterior midline of the parietals (Figures 4a, 8a, 9a). The Effigia large-beaked cranium model displays similar distributions of von Mises stress to the small-beaked model although the former displays slightly lower stress around the quadrates, squamosals, parabasisphenoid and posterior midline of the parietals (Figures 4b, 8a, 9a). The small-beaked mandible model displays very high von Mises stress distributions across most of the surangular and the ventral surface of the angular (Figure 4c). The large-beaked mandible model displays very similar stress distributions to the small-beaked mandible model except that the rhamphotheca exhibits much lower stress than the equivalent exposed bone in the small beak model (Figure 4c,d).

The *Ornithomimus* small-beaked cranium model displays very low stresses across the cranium with only the ventral and lateral surfaces of the quadrates, the lateral surfaces of the pterygoids and parietals, and the

posterolateral surface of the parabasisphenoid showing small areas of intermediate stress (Figures 4e, 8a, 9a). The Ornithomimus large-beaked cranium model displays very similar stress distributions to the small-beaked model except that the large-beaked model displays more restricted areas of elevated stress around the parietals and ventral surfaces of the quadrates (Figures 4e,f, 8a, 9a). Struthio displays very high stresses across: most of the pterygoids and palatines; the anterior surface of the parabasisphenoid; the dorsal surfaces of the jugals and the lateral surfaces of the quadrates (Figures 4g, 8a, 9a). Alligator generally exhibits relatively low stresses across the cranium (Figures 4h, 8a, 9a). Areas of high stress include: the nasal bridge; the ventral surfaces of the maxilla in between the maxillary teeth; the lateral and ventral surfaces of the pterygoids and the medial surface of the quadrates (Figure 4h).

During middle bite simulations, the Effigia smallbeaked cranium model displays similar stress distributions to the anterior bite simulation, with high stresses around the squamosals, quadrates, pterygoids, parabasisphenoid and the ventral surface of the parietals (Figures 5a, 8b, 9b). However, the middle bite simulation exhibits lower stress around the nasal bridge and higher stress on the medial surfaces of the maxillae (Figures 5a, 8b, 9b). The Effigia large-beaked cranium model displays broadly similar stress distributions to the anterior bite simulation (Figures 5b, 8b, 9b) but the nasal bridge exhibits much lower stresses (Figures 5b, 8b, 9b). The Effigia small-beaked mandible model displays similar distributions of very high stress to that of the anterior bite simulation, although in the former there are larger areas of very high stress in the ventral and dorsal surfaces of the surangular and angular, respectively (Figure 5c). The Effigia large-beaked mandible model displays larger areas of very high stress across the surangular than the anterior bite simulation (Figure 5c,d). For both the small- and large-beaked Ornithomimus model middle bite simulations, the stress distributions during middle biting are almost identical to those observed in the anterior bite simulations (Figures 4e,f, 5e,f, 8a, 9a). Middle bites in Struthio generate very similar stress distributions to the anterior bite simulation with the exceptions that the former displays slightly higher stress around the posterior half of the jugal and slightly lower stress around the nasal bridge and palatal surface of the vomers (Figures 5g, 8b, 9b). Alligator displays low stresses across the cranium during middle biting (Figures 5h, 8b, 9b). The ventral surfaces of the pterygoids and of the maxillae between the maxillary teeth exhibit slightly lower stress than the anterior bite simulation (Figures 5h, 8b, 9b).

During posterior bite simulations, the *Effigia* small-beaked cranium model displays higher stress around the

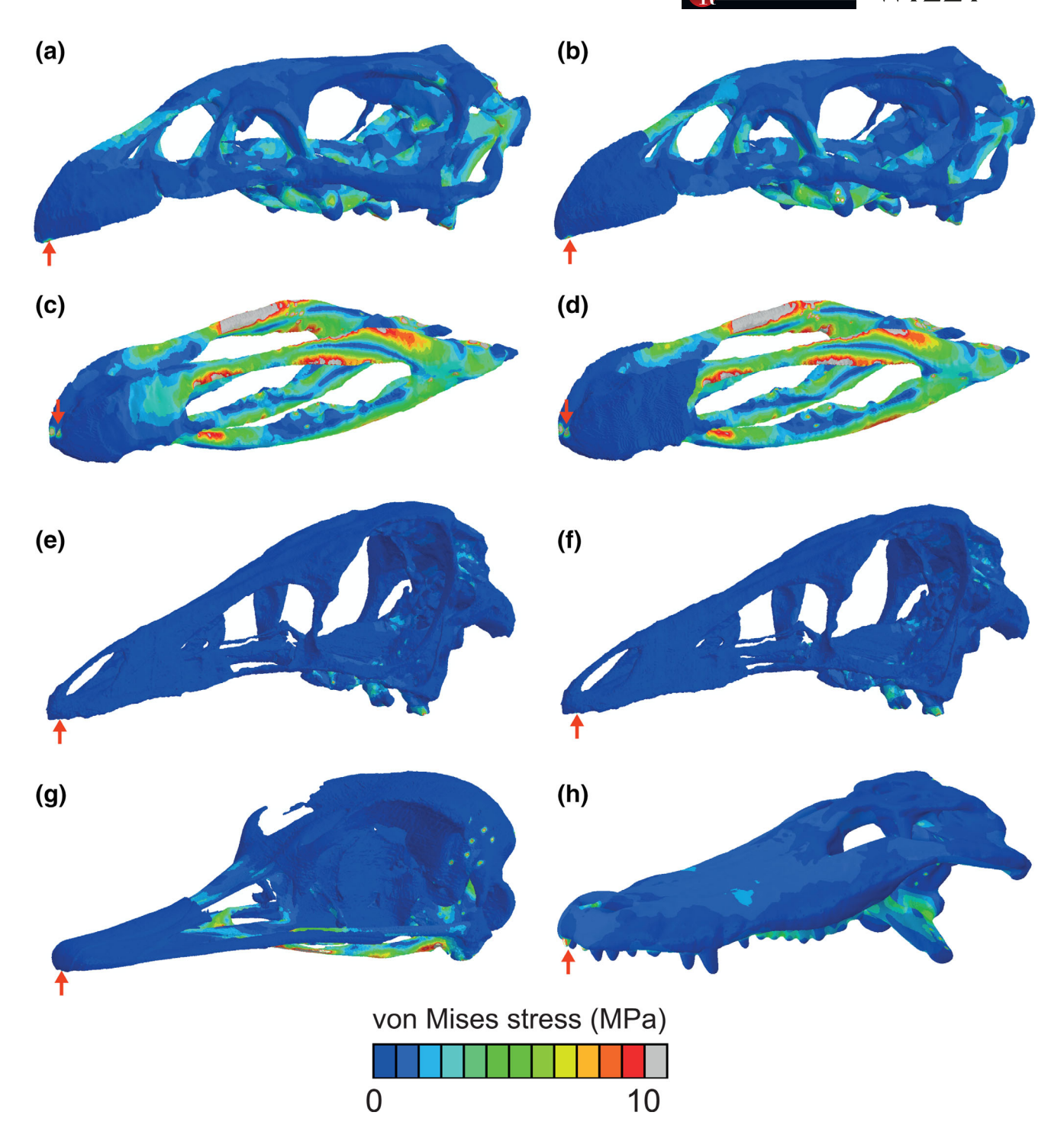


FIGURE 4 Comparisons of von Mises stress distribution of study taxa subjected to bilateral anterior bite simulations. (a) small-beaked Effigia okeeffeae cranium, (b) large-beaked Effigia cranium, (c) small-beaked Effigia mandible, (d) large-beaked Effigia mandible, (e) small-beaked Ornithomimus edmontonicus cranium, (f) large-beaked Ornithomimus cranium, (g) Struthio camelus cranium, (h) Alligator mississippiensis cranium. Bite positions indicated by red arrows (only one side of jaw is indicated for clarity). Models were all scaled to the same surface area, and muscle loads scaled accordingly, for analysis. Scaling information can be found in Table 1. All models are shown in oblique view

dorsal surface of the palatines, the posterior surfaces of the maxillae, the anterior surfaces of the lacrimals and the parabasisphenoid than in the other bite simulations (Figures 6a, 8c, 9c). The medial surfaces of the maxillae display lower stress (Figures 6a, 8c, 9c). The *Effigia* large-beaked cranium model displays larger areas of high stresses than the other bite simulations, including in the maxillae, lacrimals and parabasisphenoid (Figures 6b, 8c, 9c).

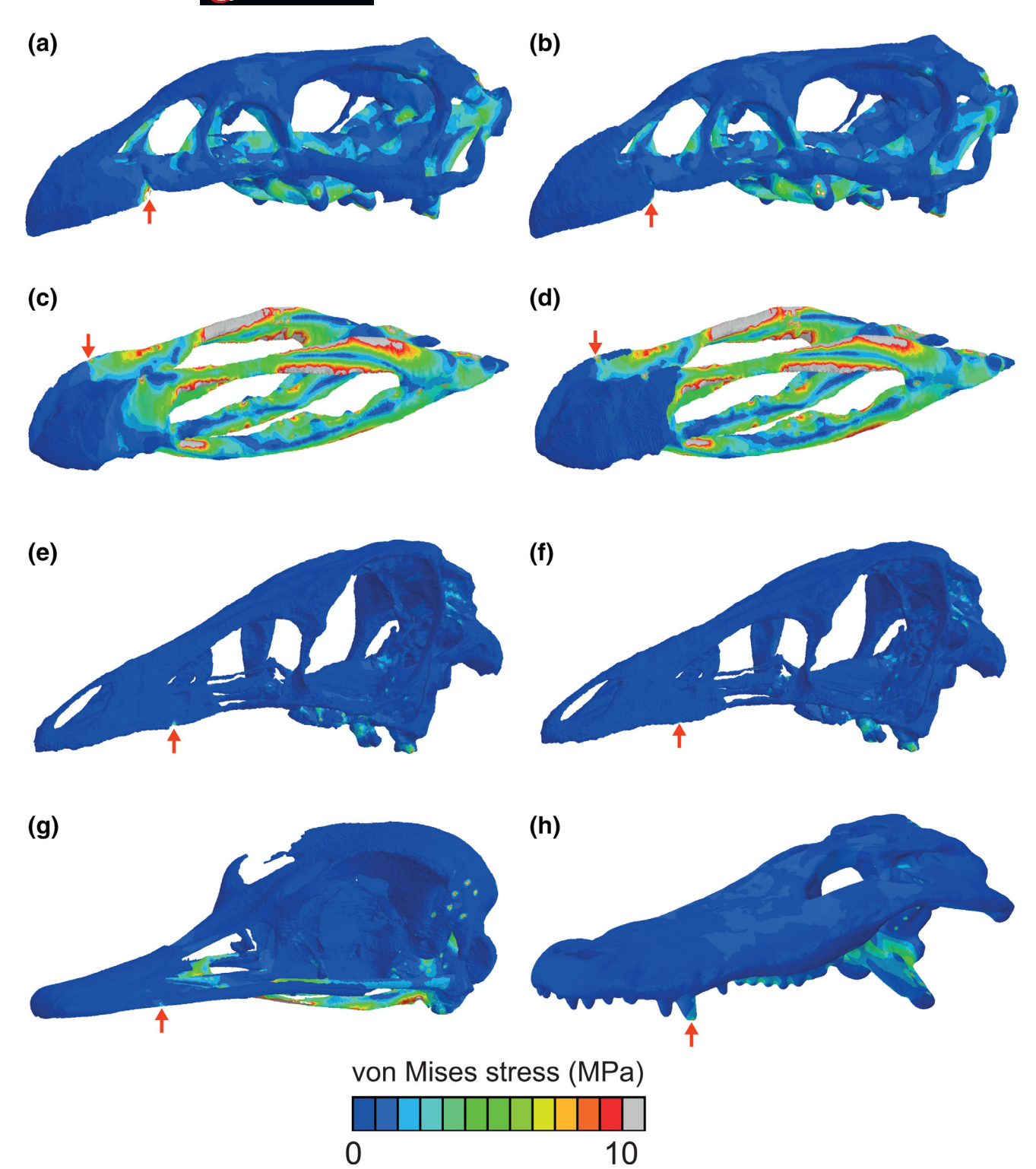


FIGURE 5 Comparisons of von Mises stress distribution of study taxa subjected to bilateral middle bite simulations. (a) small-beaked Effigia okeeffeae cranium, (b) large-beaked Effigia cranium, (c) small-beaked Effigia mandible, (d) large-beaked Effigia mandible, (e) small-beaked Ornithomimus edmontonicus cranium, (f) large-beaked Ornithomimus cranium, (g) Struthio camelus cranium, (h) Alligator mississippiensis cranium. Bite positions indicated by red arrows (only one side of jaw is indicated for clarity). Models were all scaled to the same surface area, and muscle loads scaled accordingly, for analysis. Scaling information can be found in Table 1. All models are shown in oblique view

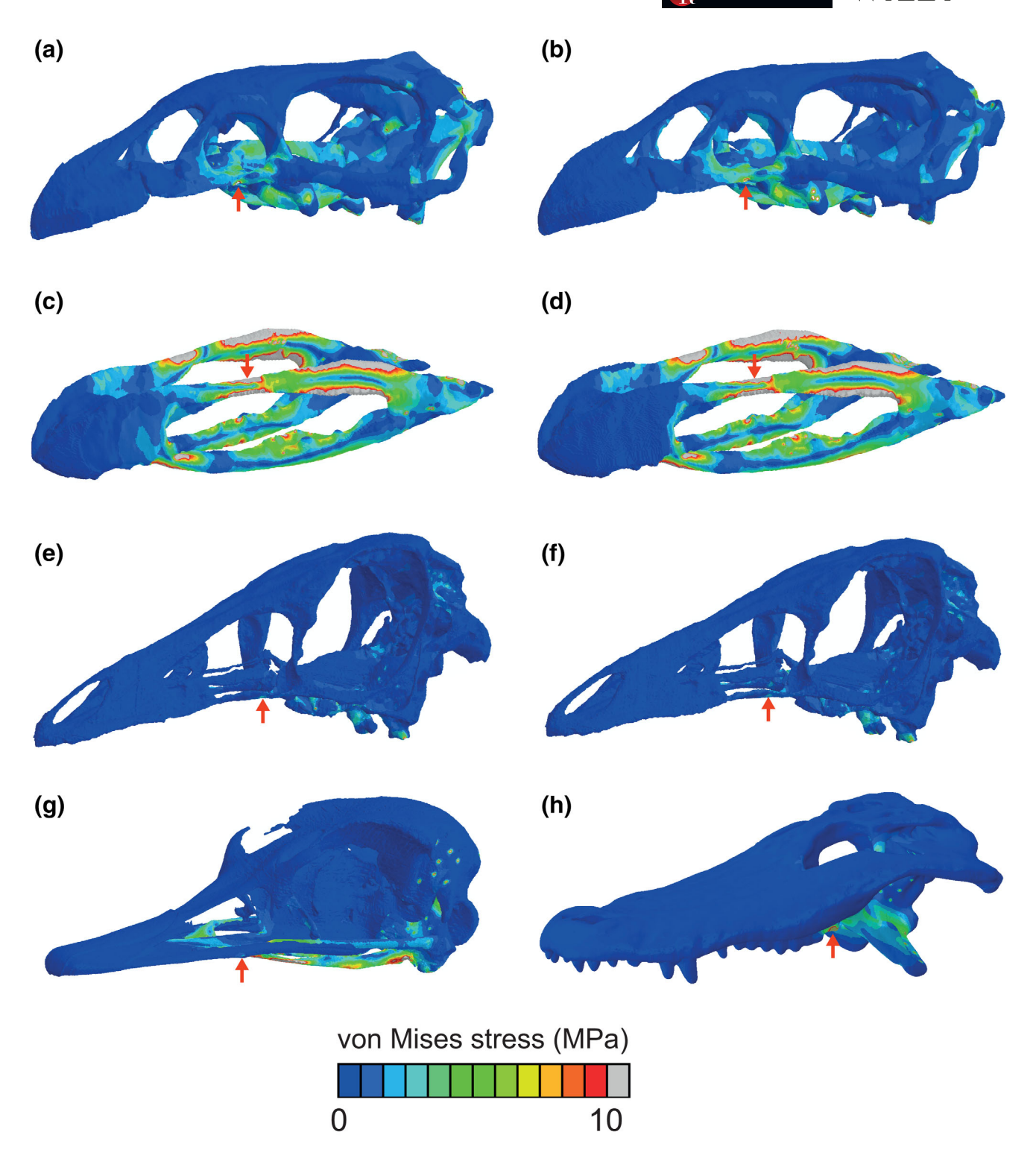


FIGURE 6 Comparisons of von Mises stress distributions of study taxa subjected to bilateral posterior bite simulations. (a) small-beaked Effigia okeeffeae cranium, (b) large-beaked Effigia cranium, (c) small-beaked Effigia mandible, (d) large-beaked Effigia mandible, (e) small-beaked Ornithomimus edmontonicus cranium, (f) large-beaked Ornithomimus cranium, (g) Struthio camelus cranium, (h) Alligator mississippiensis cranium. Bite positions indicated by red arrows (only one side of jaw is indicated for clarity). Models were all scaled to the same surface area, and muscle loads scaled accordingly, for analysis. Scaling information can be found in Table 1. All models are shown in oblique view

The *Effigia* small-beaked mandible model displays large areas of very high stress around the surangular and angular, although stresses in the anterior half of the mandible

are lower than in the other bite simulations (Figure 6c). The *Effigia* large-beaked mandible model displays very high von Mises stresses that are similar to the

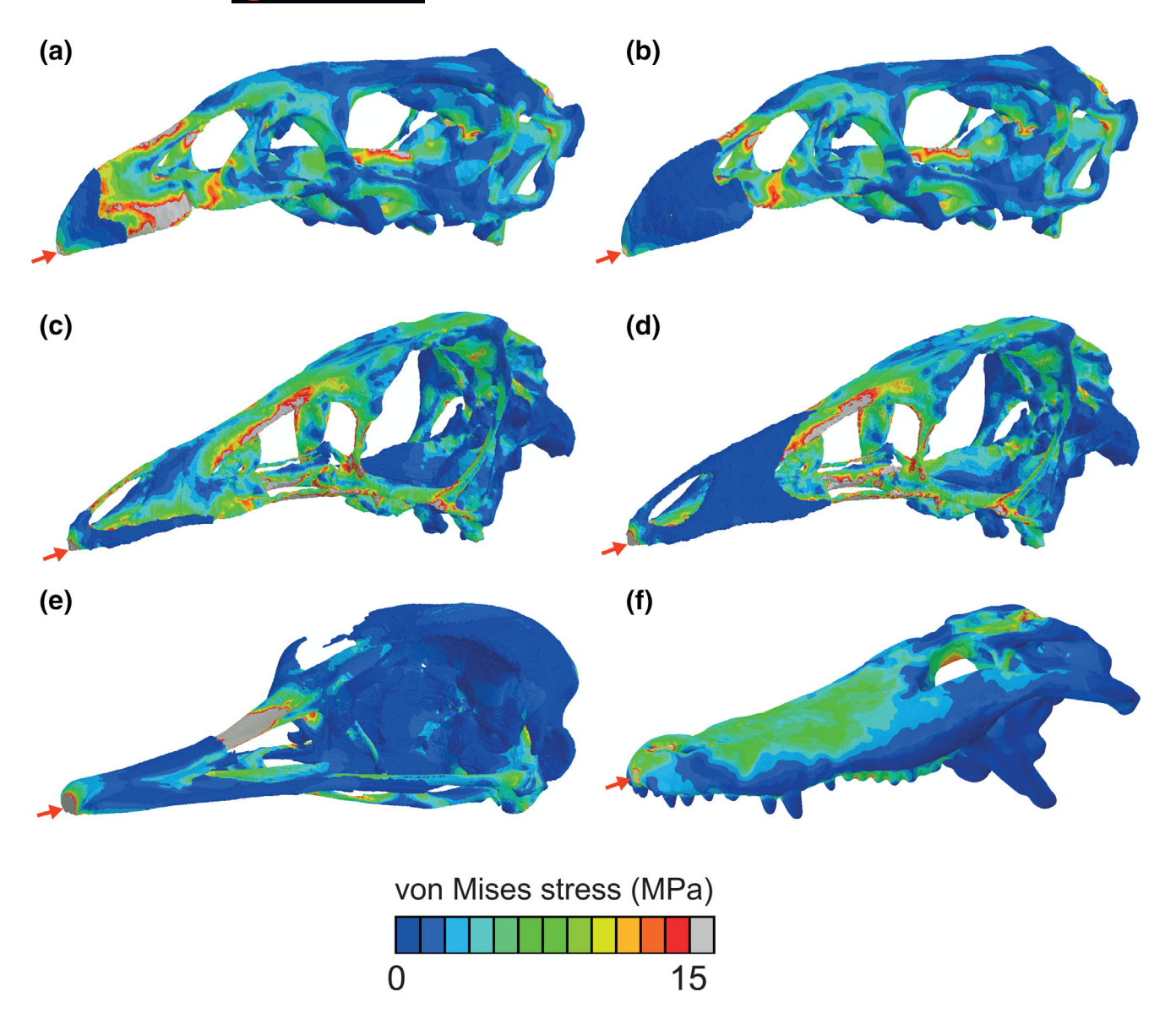


FIGURE 7 Comparisons of von Mises stress distributions of study taxa subjected to pecking simulations. (a) small-beaked *Effigia* okeeffeae cranium, (b) large-beaked *Effigia* cranium, (c) small-beaked *Ornithomimus edmontonicus* cranium, (d) large-beaked *Ornithomimus* cranium, (e) *Struthio camelus* cranium, (f) *Alligator mississippiensis* cranium. The location and direction of the loading force is indicated by the red arrows. Note the different scaling for stress compared to the biting simulations (Figures 4–6). Models were all scaled to the same surface area for analysis. Scaling information can be found in Table 1. All models are shown in oblique view

distributions of the small-beaked mandible model posterior bite simulation (Figure 6c,d). For both the small-and large-beaked *Ornithomimus* models, the stress distributions are very similar to those displayed in the anterior and middle bite simulations (Figures 4e,f, 5e,f, 6e,f, 8, 9). *Struthio* displays very similar stress distributions to the anterior and middle bite simulation (Figures 4g, 5g, 6g, 8, 9). *Alligator* displays generally little stress across the cranium; the ventral surface of the pterygoids displays the highest stresses, although the lateral surfaces of these bones display less stress

than in other bite simulations (Figures 4h, 5h, 6h, 8c, 9c).

During pecking simulations, the *Effigia* small-beaked cranium model displays very high stresses in most regions, including: areas of the premaxillae not covered by the rhamphotheca; the anterior-most tip of the premaxillae, the nasal bridge; the anterior and medial surfaces of the maxillae; the lateral and dorsal margins of the parabasisphenoid; the anterior surfaces of the squamosals; and dorsal and palatal midline of the parietals (Figures 7a, 8d, 9d). The *Effigia* large-beaked cranium

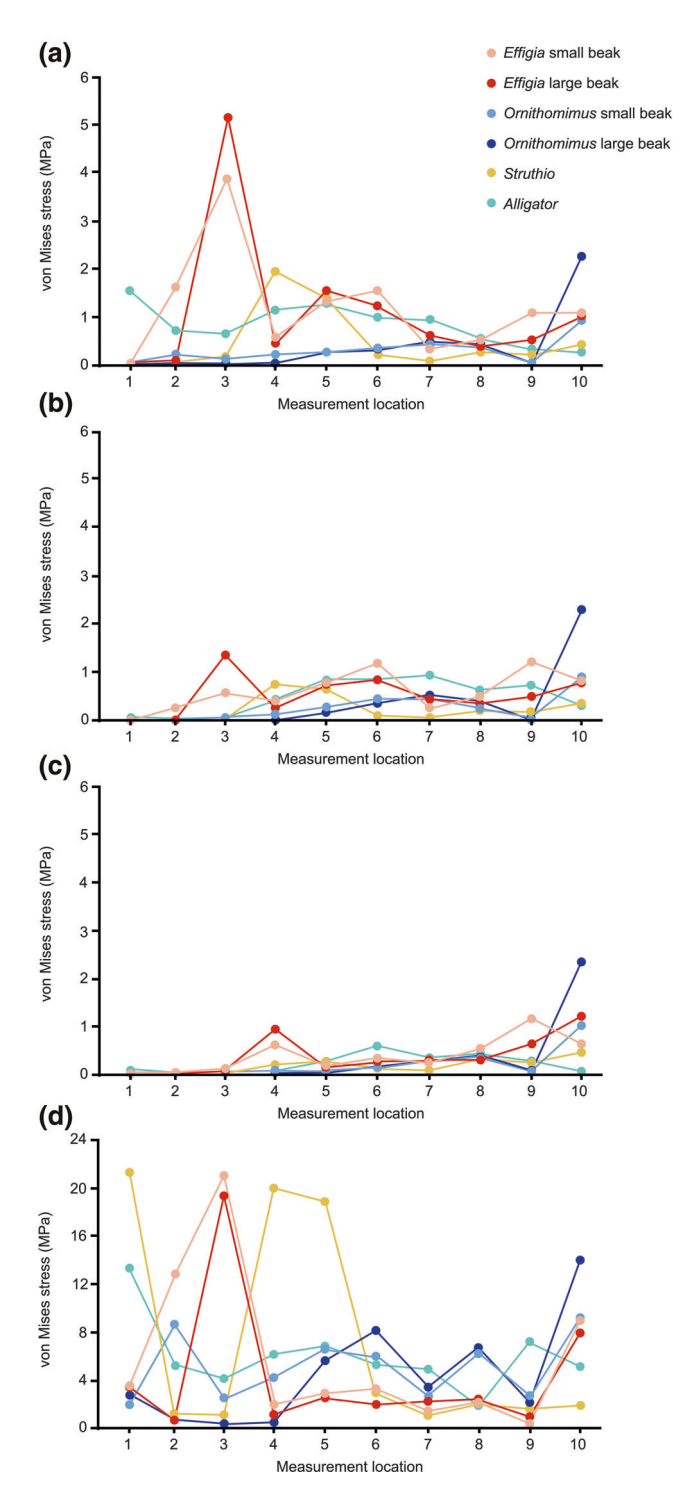


FIGURE 8 von Mises stress magnitudes of the of the study archosaur crania at 10 measurement locations along their dorsal surfaces for four different feeding simulations. (a) bilateral anterior bite simulation values, (b) bilateral middle bite simulation values, (c) bilateral posterior bite simulation values, (d) pecking simulation values. Note the different y-axis scales between (a-c) and (d). Measurement point locations along each cranium can be found in Figure S2

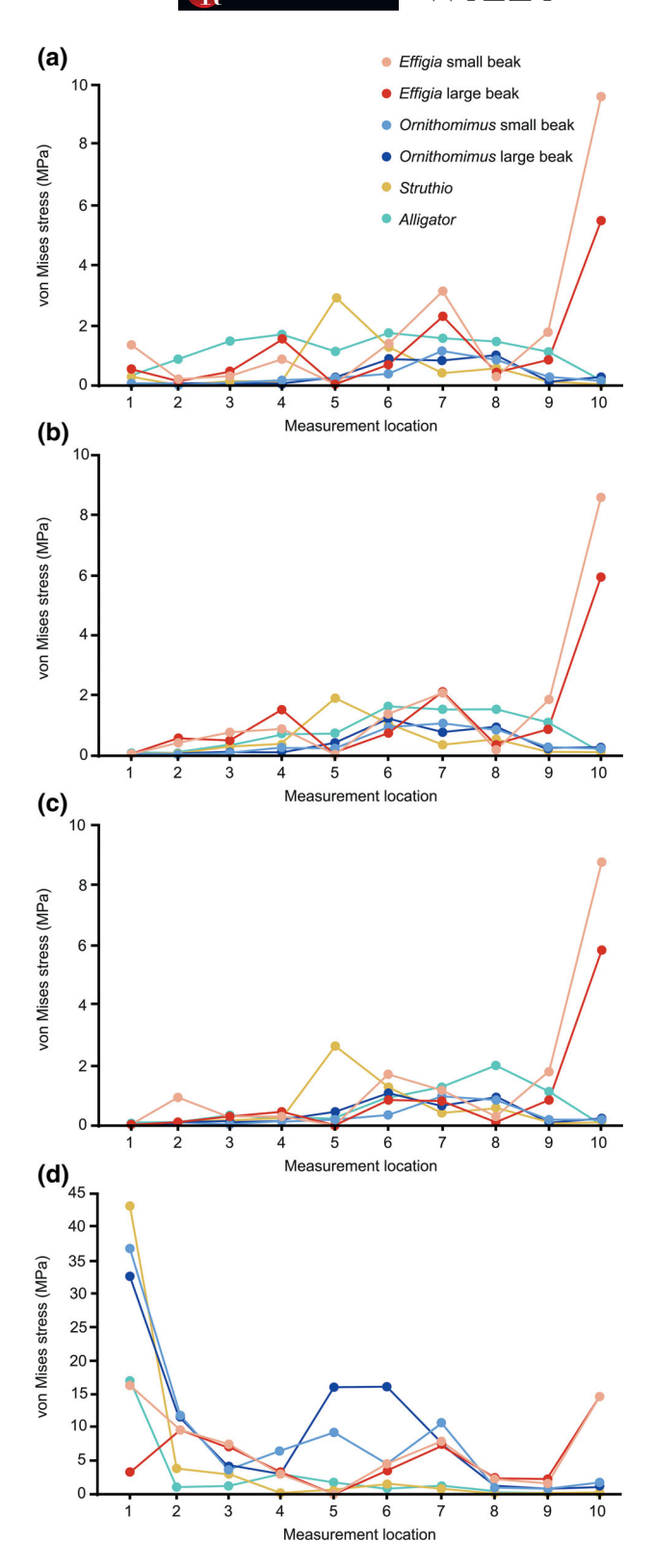


FIGURE 9 von Mises stress magnitudes of the of the study archosaur crania at 10 measurement locations along their palatal surfaces for four different feeding simulations. (a) bilateral anterior bite simulation values, (b) bilateral middle bite simulation values, (c) bilateral posterior bite simulation values, (d) pecking simulation values. Note the different y-axis scales between (a–c) and (d). Measurement point locations along each cranium can be found in Figure S2

model has comparable stress distributions to the smallbeaked model. The main difference is that the larger rhamphotheca displays much lower stress levels in the dorsal and palatal surfaces than the equivalent areas of exposed premaxillae and maxillae in the small-beaked model (Figures 7a,b, 8d, 9d). The Ornithomimus smallbeaked cranium model displays very high von Mises stresses concentrated in: the nasal bridge; the lateral and palatal surfaces of the maxillae; the palatal surface of the vomers and basisphenoid; and the lacrimals and posterior surfaces of the jugals (Figures 7c, 8d, 9d). The Ornithomimus large-beaked cranium model displays somewhat similar stress distributions to the small-beaked model, the main differences being that the larger rhamphotheca displays much lower stress in the largebeaked simulation than the uncovered premaxillae and maxillae in the small-beaked simulation, while the palatal surface of the vomers and dorsal surface of the parietals exhibit higher stresses in the large-beaked model (Figures 7c,d, 8d, 9d). Struthio displays several areas of very high stresses across the cranium during pecking, including: the anterior surface of the rhamphotheca; areas of the nasals that are not covered by the rhamphotheca; the anterior halves of the pterygoid; the parasphenoid; the quadratojugal; and the dorsal surfaces of the quadrates (Figures 7e, 8d, 9d). Alligator generally exhibits high stresses across most of the cranium, including: the dorsal and ventral surfaces of the premaxillae, including the nasal bridge; the dorsal surfaces of the maxillae and the ventral surface between the maxillary teeth; the parietals; the postorbitals; and the posterior surface of the jugals that border the lateral temporal fenestrae (Figures 7f, 8d, 9d). By contrast, except for the anteriormost tip of the premaxillae, the palatal surface of the Alligator cranium exhibits lower stresses than most of the other models (Figure 9d).

4 | DISCUSSION

4.1 | Morphological convergence between Effigia and "ostrich-like" avemetatarsalians

The *Effigia* skull reconstruction presented here reaffirms many of the characters cited as morphological convergences between this pseudosuchian taxon and ornithomimid dinosaurs, including enlarged orbits and edentulous jaws (Nesbitt, 2007; Nesbitt & Norell, 2006), and the ventral deflection of the anterior tip of the dentaries. However, we identify four marked differences between *Effigia* and "ostrich-like" avemetarsalians. (a) The proportions of the *Effigia* rostrum are

anteroposteriorly shorter and mediolaterally broader in relation to overall cranium length, especially in comparison to those of ornithomimids. In addition, the ventrally concave margins of the Effigia premaxillae enables contact between the entire length of the dorsomedial and dorsolateral surfaces of the premaxillae and dentaries, a unique condition among the taxa studied herein. (b) In Effigia, the external nares are much larger in lateral view than in either of the avemetatarsalian taxa, are located more posteriorly than in Ornithomimus, and differ in having a more triangular outline. (c) In Effigia the nasal bridge is slightly concave whereas in Struthio it is strongly concave and in Ornithomimus it is convex. (d) The Effigia mandible is dorsoventrally taller than that of the other study taxa and is perforated by a huge external mandibular fenestra. Morphological differences like these are often not considered as strongly as morphological similarities when inferring functional convergence between unrelated taxa (Lauder, 1995), which often results in mismatches between hypothesized function based on comparative anatomy alone versus that inferred from quantitative biomechanical modeling (Bestwick et al., 2018).

4.2 | Biomechanical modeling comparisons

Overall, the muscle reconstructions and FEA outputs indicate that the skull of Effigia possesses a unique mosaic of mechanically strong and weak features for its size (around 2 m long total length and 1 m tall total height (Nesbitt, 2007); no mass estimates yet available). For example, the large cross-sectional areas of the jawclosing muscles and relatively high estimates of muscle force, in particular that for the m. PTv, are perhaps unsurprising given the extremely large diameter of the cranial and mandibular fenestrae, which can potentially provide extensive surfaces for muscle attachment sites (Holliday, 2009; Pêgas et al., 2021). However, the occurrence of high magnitude stresses in the mandibles and nasal bridge highlight these areas as mechanically weak. This indicates that the jaw muscles may not have exerted forces close to the maximum values calculated in this study during feeding.

The impact of reconstructed rhamphotheca morphology on stress distributions is clearly demonstrated, particularly in the anterior biting and pecking simulations. The large-beaked morphology is more effective at dissipating stresses around the premaxillae and nasal bridges (except for areas not covered by the rhamphotheca), and around the dentary. Similar results have been reported from investigations on rhamphotheca function in extant birds

and non-avian dinosaurs (Cuff et al., 2015: Lautenschlager et al., 2013; Soons et al., 2012), highlightfunctional convergence between beaked avemetatarsalians and Effigia. We do not draw any conclusions on the actual shape and thickness of the Effigia rhamphotheca as that was not a primary aim of this study. We simply infer, based on our results, that larger cranial and mandibular rhamphothecae would have enabled better dissipation of high stresses generated during feeding behaviors.

Model comparisons between Effigia and Ornithomimus are somewhat limited due to the cautious approach taken with respect to muscle reconstructions of the latter (Cuff & Rayfield, 2015). Although we accept that ornithomimids had disproportionately small jaw muscles and weak bites for their size (Cuff & Rayfield, 2015), these conservative estimates likely resulted in the low stress distributions presented here, artificially indicating a strong cranium. Nevertheless, useful comparisons can be made. For example, extremely high stress magnitudes from the pecking simulations in both taxa are unsurprising since their crania do not exhibit functional kinesis and thus lack a mechanism to facilitate more uniform stress distributions (Cuff et al., 2015; Curtis et al., 2013; Moazen et al., 2013; Rayfield, 2007). However, differences in the distribution of high magnitude stresses are important for inferring the relative likelihoods of this behavior. In Effigia, most of the high magnitude stresses are in the anterior third of the cranium and are partially dissipated by the rhamphotheca in the large-beaked model. In contrast, most of the high magnitude stresses in Ornithomimus are in the posterior twothirds of the cranium. Less stress is therefore dissipated in the Ornithomimus large beak model compared to the Effigia large beak model. While 340 N is a high upper estimate of external force, pecking behaviors nonetheless result in high, potentially detrimental stress for both taxa. This result is unexpected given the degree of morphological convergence between ornithomimids and palaeognaths (Barrett, 2005; Makovicky et al., 2004), which further exemplifies the notion that shared form does not necessarily reflect similar function in extinct taxa (Ferry-Graham et al., 2002; Fisher, 1985; Lautenschlager et al., 2016; Thomason, 1995).

The Struthio FEA outputs demonstrate the functional differences between it and the extinct edentulous taxa in this study. The location of the adductor muscle origins in the ventral half of the cranium is a derived condition for Aves, due primarily to expansion of the braincase (Holliday & Witmer, 2007; Jones et al., 2019; Lautenschlager et al., 2014), which results in low magnitude stress distributions around the dorsal half of the cranium. The biting simulations also highlight the palate as the main area of structural weakness, reflecting the fact

that Struthio does not use orthal biting motions to procure or process food items (Milton et al., 1994; Williams et al., 1993). The relatively large pterygoideus muscles instead serve to mitigate mandibular retraction from the adductors (Gussekloo & Bout, 2005a). Struthio feeds primarily by plucking small grasses, flowers, leaves and fruits from the ground or low-lying plants, and throwing these items to the back of the jaws to be swallowed (Milton et al., 1994; Williams et al., 1993). This feeding behavior is informally termed "catch-and-throw behavior" (Zweers et al., 1994). Much of the external force associated with feeding is therefore focused around the anterior-most part of the rostrum as the bill regularly contacts the ground while plucking, while the palate is subjected to much lower forces. Our pecking simulations better replicate this behavior, so it is unsurprising that Struthio exhibits generally low magnitude stress distributions in our simulations. It should be noted that stresses in the nasal bridges are artificially high due to the removal of sutural bone from this area which is known to mitigate stress (Cuff et al., 2015). Nevertheless, features for pecking behaviors appear to be unique to Struthio among our study taxa and casts doubt on distantly related "ostrich-like" archosaurs exhibiting identical suites of functional behaviors.

The Alligator FEA outputs demonstrate clear morphological and functional differences between it and Effigia. The dorsoventrally flattened skulls of extant crocodylians are widely regarded as adaptations for semiaquatic life (Grigg & Kirshner, 2015; Iordansky, 1973; McHenry et al., 2006), and the extended pterygoid flanges provide enlarged attachment sites for the adductor muscles (Holliday et al., 2013, 2015; Sellers et al., 2017). Crocodylians exhibit the largest bite forces among extant tetrapods (Erickson et al., 2003, 2012), and our results are consistent with previous biomechanical studies showing that crocodylian skulls are adapted to resist high feedinggenerated forces (McHenry et al., 2006; Montefeltro et al., 2020; Walmsley et al., 2013). This capacity enables extant crocodylians to occupy durophagous and/or apex predator niches (see Somaweera et al., 2020 for a review). The anterior bite simulation highlights the nasal bridge as mechanically weak in Alligator, as in Effigia, although crocodylians mitigate stresses in this area by using unilateral bites to seize prey (Erickson et al., 2012; Montefeltro et al., 2020), and crushing items in the posterior region of the jaws before swallowing (Cleuren & De Vree, 2000; Labarre et al., 2017). The high magnitude stresses from the pecking simulation are expected since crocodylian skulls are akinetic (Sellers et al., 2017) and so possess no morphological adaptations to dissipate these stresses, suggesting that such a feeding behavior is not possible. The functional morphology of *Alligator*

adaptations for a very different lifestyle from that proposed for *Effigia*.

4.3 | Possible feeding behaviors of Effigia

The morphological and functional evidence presented here and in previous studies suggests that Effigia was most likely adapted for herbivory (Button & Zanno, 2020; Lautenschlager et al., 2016; Nesbitt, 2007; Nesbitt & Norell, 2006; Zanno & Makovicky, 2011). Consequently, further questions relating to the ecology and functional morphology of Effigia concern the types of plant material consumed and the feeding behaviors used to acquire them. As previously mentioned, pecking behavior was possible but likely limited. The mechanically weak mandible probably restricted food procurement processing to the anterior portion of the jaws. It is unlikely that Effigia crushed hard food objects with its rostrum due to the weak nasal bridge and the low mechanical advantage when processing foods further away from the jaw musculature and craniomandibular joint (Erickson et al., 2012; Kammerer et al., 2006; Santana et al., 2010; Santana & Dumont, 2009), although the swallowing of small seeds that require no processing cannot be excluded.

An alternative feeding behavior involves occlusion between the surfaces of the dorsoventrally concave rostrum and ventrally deflected anterior mandible. This bite would have enabled a shear-like cropping motion as the bite point moves anteriorly along the ventromedial and dorsolateral surfaces of the premaxillae and dentaries during jaw closure. Cropping behaviors generate less stress on the jaws than crushing behaviors (Jasinoski et al., 2009), which may have facilitated consumption of relatively fibrous plant matter. This behavior would be more likely if the rhamphothecae were large, as their presence would dissipate stresses along more of the occlusal surfaces of the premaxillae and dentaries. However, the overall weakness of the mandible suggests that if cropping was the main feeding behavior, Effigia would likely prioritize soft plants or softer plant parts. Further testing of the speed of Effigia jaw closure could reveal more information on the efficiency of cropping behaviors.

Other feeding behaviors associated with herbivory could have been used by *Effigia* but require further investigation. For example, the catch-and-throw behavior used by extant palaeognaths (Dzemski & Christian, 2007; Gussekloo & Bout, 2005b; Zweers et al., 1994) is theoretically possible as a ventrally deflected anterior portion of the mandible provides a larger, scoop-like surface for procuring items from the ground. However, palaeognaths

have highly flexible cervical vertebrae that enable the head to reach down and pluck items from the ground (Dzemski & Christian, 2007), and extrapolating neck flexibility to extinct taxa requires thorough understanding of the soft tissues in the neck (Cobley et al., 2013). The current lack of rigorous cervical muscle reconstructions in *Effigia* therefore limits our understanding of the potential role of the neck in feeding behavior.

Another possible behavior involves stripping plant material from branches by recruiting the neck muscles to pull the skull posteriorly while the jaws are closed. This behavior is used by some extant birds that possess dorsoventrally tall mandibles, such as vultures (Accipitridae) to remove flesh from carcasses (Hertel, 1995). Moreover, pull-back behaviors have been suggested for herbivorous therizinosaurid dinosaurs, as the simultaneous use of the jaw and anterior neck muscles subjects the cranium to lower stresses than the jaw muscles acting alone (Lautenschlager et al., 2013). However, poor preservation of the *Effigia* braincase (Nesbitt, 2007) prevents accurate reconstructions of the craniocervical joint and musculature at present.

4.4 | Functional and ecological convergence between pseudosuchians and avemetatarsalians

Our biomechanical modeling demonstrates that the functional morphology of *Effigia* is unlike that of either "ostrich-like" avemetatarsalians or crocodylians. This



FIGURE 10 Life reconstruction of *Effigia okeeffeae* based on the skull redescription and results of the functional models. *Effigia* is depicted feeding on softer plant material, represented by the fern-like *Cladophlebis* from the Chinle Formation (Parker & Martz, 2010). Created by Mark Witton, who retains the copyright

study thereby emphasizes the finding that the repeated evolution of similar bauplans in distantly related taxa does not automatically imply functional and ecological convergence, and that quantitative biomechanical modeling techniques should be used where possible to test such hypotheses (Bestwick et al., 2018; Lauder, 1995; Lautenschlager et al., 2016). Greater consideration of the environmental conditions and evolutionary histories of morphologically convergent taxa are also needed in order to understand the likelihood of ecological and functional convergence. For example, ostriches are opportunistic herbivores that feed almost exclusively on low-lying angiosperms such as grasses and shrubs (Williams et al., 1993), plants that were not present in the Triassic. Furthermore, stress distribution differences between our study pseudosuchians probably reflect the \sim 245 million years of independent evolutionary history between Effigia and Alligator (Brusatte et al., 2010; Nesbitt, 2011), with crocodylians undergoing marked morphological changes for adaptation to inhabit aquatic habitats (Grigg & Kirshner, 2015; Iordansky, 1973). However, it is possible that some phylogenetic signal would have been present when considering more closely related pseudosuchian clades. Phylogenetic relationships within Poposauroidea are relatively well resolved with its constituent lineages exhibiting remarkably high morphological disparity (Butler et al., 2011; Nesbitt, 2011; Schachner et al., 2019). The sister taxon of the gracile, bipedal and edentulous shuvosaurids is Lotosaurus, a taxon with edentulous jaws and large external nares, which is a robust quadruped with a distinct dorsal sail (Butler et al., 2011; Nesbitt, 2011; Zhang, 1975). The next most inclusive taxon is Poposaurus, a gracile biped that shares many morphological similarities with early diverging theropod dinosaurs, such as recurved teeth (Mehl, 1915; Nesbitt, 2011; Parker & Nesbitt, 2013). The order in which poposauroid bauplans were assembled and/or modified is currently unclear (Nesbitt, 2011). This evidence indicates that the anatomy and functional morphology of shuvosaurids is more likely the result of shared ancestry and rapid experimentation (Stocker et al., 2016), rather than similar selection pressures acting on both shuvosaurids and ostrich-like avemetatarsalians.

Our results, in tandem with morphological data and functional investigations of other contemporaneous archosaurs suggest that *Effigia*, and by extension other shuvosaurids, performed unique functional and ecological roles within Late Triassic terrestrial ecosystems and were likely selective herbivores that fed primarily by browsing on soft plants/softer plant parts (Figure 10). While there is no direct evidence on the plants that might have formed shuvosaurid diets, new growth from extant plants is structurally weak due to low silica and lignin

content (Massey et al., 2007). It is therefore possible that shuvosaurids prioritized feeding on new plant growth. In the absence of detailed information on neck function, shuvosaurids are likely to have fed within 1-2 m of ground level (Figure 10; upper estimate based on incomplete Sillosuchus material; Nesbitt, 2011). This result contrasts some contemporaneous aetosaurs such Stagonolepis and Typothorax, whose robust limbs, shovelshaped rostra and high bite forces suggest diets of tough vegetation located underground (Desojo et al., 2013; Desojo & Vizcaíno, 2009; Heckert et al., 2010) (but see Taborda et al., 2021 for suggestions of possible faunivory in a Late Triassic aetosaur from 3D finite element analysis). In addition, biomechanical studies of sauropodomorphs suggest they were generalized herbivores, perhaps exhibiting facultative faunivory (Button et al., 2016; Lautenschlager et al., 2016), and likely fed on taller plants based on their larger body size (Galton, 1985). Overall, our results suggest that Late Triassic food webs were more functionally diverse and complex than previously appreciated.

5 | CONCLUSIONS

Our study shows that despite the high degree of overall similarity between the crania of Effigia, ornithomimids and extant palaeognaths, the functional morphology of this pseudosuchian differed substantially from that of "ostrich-like" archosaurs. Effigia possesses an unusual mosaic of mechanical features that most likely restricted habitual feeding functions to the anterior portion of its jaws. A shearing motion between the anterior parts of the mandible and rostrum during orthal closure would have generated the least stress under our modeling conditions. Our analyses indicate that this pseudosuchian was most likely herbivorous and likely a specialist that cropped the softer parts of plants during feeding. Our study indicates that although "ostrich-like" bauplans evolved independently at least three times in archosaurs over a 230-million-year period, different functional behaviors were employed by each lineage. This study showcases the importance of rigorous, quantitative and repeatable techniques like FEA to deduce whether morphological convergence between unrelated taxa confers functional convergence or not as well as providing the potential to uncover more detailed information on their specific ecological roles. The inferred functional morphology of Effigia indicates that it (and other closely related and morphologically similar shuvosaurids) performed a unique ecological role within Late Triassic food webs. This example not only increases our understanding of Late Triassic terrestrial ecosystems, but also emphasizes the overall

ecological diversity and success of the pseudosuchian archosaurs at this time.

ACKNOWLEDGMENTS

We thank Casey Holliday and Emma Schachner for the invitation to contribute to this special issue. Thanks to Mark Witton for creating the life restoration in Figure 10. Thanks to Luke Meade for useful advice on using Avizo and Hypermesh. This work started as an MSc project by A.S.J. and was completed with support from a Leverhulme Trust Research Project Grant (RPG-2019-364) to R.J.B, S.L., P.M.B. and L.B.P. S.J.N. was supported by a National Science Foundation (US) CAREER grant (EAR 1943286).

CONFLICT OF INTEREST

We declare no competing interests.

AUTHOR CONTRIBUTIONS

Jordan Bestwick: Formal analysis (equal); investigation (equal); methodology (equal); project administration (lead); visualization (lead); writing – original draft (lead); writing – review and editing (lead). Andrew Jones: Data curation (equal); formal analysis (equal); investigation (equal); methodology (equal); writing - original draft (supporting); writing - review and editing (supporting). **Sterling Nesbitt:** Conceptualization (lead); curation (equal); funding acquisition (equal); visualization (supporting); writing - original draft (supporting); writing - review and editing (supporting). Stephan Lautenschlager: Conceptualization (equal); curation (lead); funding acquisition (supporting); project administration (supporting); resources (lead); software (lead); supervision (equal); visualization (supporting); writing – original draft (supporting); writing – review and editing (supporting). Emily Rayfield: Conceptualization (lead); project administration (supporting); resources (equal); software (equal); supervision (equal); writing – original draft (supporting); writing – review and editing (supporting). Andrew Cuff: Data curation (equal); investigation (supporting); resources (equal); visualization (equal); writing original (supporting); writing – review and editing (supporting). **David Button:** Project administration (supporting); supervision (supporting); writing - original draft (supporting); writing – review and editing (supporting). Paul Barrett: Funding acquisition (supporting); supervision (supporting); writing - original draft (supporting); writing – review and editing (supporting). Laura Porro: Funding acquisition (supporting); supervision (supporting); writing - original draft (supporting); writing - review and editing (supporting). Richard Butler: Conceptualization (lead); funding acquisition (lead);

project administration (lead); supervision (equal); writing – original draft (supporting); writing – review and editing (supporting).

ETHICS STATEMENT

No ethics approval was needed for this study. No such consent was needed for this study. We have permission to reproduce material from other sources, such as images and 3D scans. We explicitly state which images and scans are sourced from previous publications and give credit and reference to these sources.

DATA AVAILABILITY STATEMENT

Measurements and calculations for *Effigia* muscle and bite forces can be found in the Supplementary Information. Scaling information for the *Ornithomimus*, *Struthio* and *Alligator* models can be found in Table 1.

ORCID

Jordan Bestwick https://orcid.org/0000-0002-1098-6286

Andrew S. Jones https://orcid.org/0000-0002-9118-5965

Sterling J. Nesbitt https://orcid.org/0000-0002-7017-

Stephan Lautenschlager https://orcid.org/0000-0003-3472-814X

Emily J. Rayfield https://orcid.org/0000-0002-2618-750X

Andrew R. Cuff https://orcid.org/0000-0001-9509-4297

David J. Button https://orcid.org/0000-0002-7404-612X

Paul M. Barrett https://orcid.org/0000-0003-0412-3000

Laura B. Porro https://orcid.org/0000-0002-0546-2381

Richard J. Butler https://orcid.org/0000-0003-2136-7541

REFERENCES

Anderson, P. S., Bright, J. A., Gill, P. G., Palmer, C., & Rayfield, E. J. (2011). Models in palaeontological functional analysis. *Biology Letters*, 8, 119–122.

Baczko, M. B. von (2018). Rediscovered cranial material of Venaticosuchus rusconii enables the first jaw biomechanics in Ornithosuchidae (Archosauria: Pseudosuchia). Ameghiniana, 55, 365–379.

Baczko, M. B. von, Taborda, J. R. A., & Desojo, J. B. (2014). First biomechanical analysis on the skull of the ornithosuchid *Riojasuchus tenuisceps* Bonaparte 1967 from the Los Colorados Formation, Late Triassic of Argentina. *Ameghiniana, Suplemento Resúmenes*, 51, 23R.

Bailleul, A. M., Witmer, L. M., & Holliday, C. M. (2017). Cranial joint histology in the mallard duck (*Anas platyrhynchos*): New insights on avian cranial kinesis. *Journal of Anatomy*, 230, 444–460.

Barrett, P. M. (2005). The diet of ostrich dinosaurs (Theropoda: Ornithomimosauria). *Palaeontology*, 48, 347–358.

Barsbold, R., & Osmólska, H. (1990). Ornithomimosauria. In D. B. Weishampel, P. Dodson, & H. Osmólska (Eds.), *The Dinosauria*. University of California Press.

- Bestwick, J., Unwin, D. M., Butler, R. J., Henderson, D. M., & Purnell, M. A. (2018). Pterosaur dietary hypotheses: A review of ideas and approaches. *Biological Reviews*, *93*, 2021–2048.
- Bona, P., & Desojo, J. B. (2011). Osteology and cranial musculature of *Caiman latirostris* (Crocodylia: Alligatoridae). *Journal of Morphology*, 272, 780–795.
- Bramble, D. M. (1974). Occurrence and significance of the Os transiliens in gopher tortoises. *Copeia*, 1974, 102–109.
- Brusatte, S. L., Benton, M. J., Lloyd, G. T., Ruta, M., & Wang, S. C. (2010). Macroevolutionary radiation of archosaurs (Tetrapoda: Diapsida). Earth and Environmental Science Transactions of the Royal Society of Edinburgh, 101, 367–382.
- Brusatte, S. L., Benton, M. J., Ruta, M., & Lloyd, G. T. (2008). Superiority, competition and opportunism in the evolutionary radiation of dinosaurs. *Science*, *321*, 1485–1488.
- Brusatte, S. L., Butler, R. J., Sulej, T., & Niedźwiedzki, G. (2009). The taxonomy and anatomy of rauisuchian archosaurs from the Late Triassic of Germany and Poland. *Acta Palaeontologica Polonica*, *54*, 221–230.
- Burton, P. J. K. (1973). Structure of the depressor mandibulae muscle in the Kokako *Callaeas cinerea*. *Ibis*, 115, 138–140.
- Busbey, A. B. (1989). Form and function of the feeding apparatus of Alligator mississippiensis. Journal of Morphology, 202, 99-127.
- Busbey, A. B. (1995). The structural consequences of skull flattening in crocodilians. In J. J. Thomason (Ed.), Functional morphology in vertebrate paleontology (pp. 173–192). Cambridge University Press.
- Butler, R. J., Brusatte, S. L., Reich, M., Nesbitt, S. J., Schoch, R. R., & Hornung, J. J. (2011). The sail-backed reptile *Ctenosauricus* from the latest Early Triassic of Germany and the timing and biogeography of the early archosaur radiation. *PLoS One*, 6, e25693.
- Button, D. J., Barrett, P. M., & Rayfield, E. J. (2016). Comparative cranial myology and biomechanics of *Plateosaurus* and *Camarasaurus* and evolution of the sauropod feeding apparatus. *Palaeontology*, 59, 887–913.
- Button, D. J., & Zanno, L. E. (2020). Repeated evolution and divergent modes of herbivory in non-avian dinosaurs. *Current Biology*, *30*, 1–11.
- Chatterjee, S. (1978). A primitive parasuchid (phytosaur) reptile from the Upper Triassic Maleri Formation of India. *Palaeontology*, 21, 83–127.
- Chen, P.-Y., Lin, A. Y. M., Seki, Y., Stokes, A. G., Peyras, J., Olevsky, E. A., Meyers, M. A., & Mckittrick, J. (2008). Structure and mechanical properties of selected biological materials. *Journal of Mechanical Behavior of Biomedical Materials*, 1, 208–226.
- Cleuren, J., & De Vree, F. (2000). Feeding in crocodilians. In K. Schwenk (Ed.), *Feeding: Form, function, and evolution in tetrapod vertebrates* (pp. 359–354). Academic Press.
- Cobley, M. J., Rayfield, E. J., & Barrett, P. M. (2013). Inter-vertebral flexibility of the ostrich neck: Implications for estimating sauropod neck flexibility. *PLoS One*, 8, e72187.
- Colbert, E. H. (1989). The Triassic dinosaur Coelophysis. *Museum of Northern Arizona Bulletin*, 57, 1–160.
- Cuff, A. R., Bright, J. A., & Rayfield, E. J. (2015). Validation experiments on finite element models of an ostrich (*Struthio camelus*) cranium. *PeerJ*, *3*, e1294.

- Cuff, A. R., & Rayfield, E. J. (2015). Retrodeformation and muscular reconstruction of ornithomimosaurian dinosaur crania. *PeerJ*, 3, e1093.
- Curtis, N., Jones, M. E. H., Evans, S. E., O'Higgins, P., & Fagan, M. J. (2009). Visualising muscle anatomy using three-dimensional computer models—An example using the head and neck muscles of *Sphenodon. Palaeontologica Electronica*, 12, 7T.
- Curtis, N., Jones, M. E. H., Evans, S. E., O'Higgins, P., & Fagan, M. J. (2013). Cranial sutures work collectively to distribute strain throughout the reptile skull. *Journal of the Royal Society Interface*, 10, 20130442.
- Davis, J. L., Santana, S. E., Dumont, E. R., & Grosse, I. R. (2010).
 Predicting bite force in mammals: Two-dimensional *versus* three-dimensional lever models. *The Journal of Experimental Biology*, 213, 1844–1851.
- Desojo, J. B., Heckert, A. B., Martz, J. W., Parker, W. G., Schoch, R. R., Small, B. J., & Sulej, T. (2013). Aetosauria: A clade of armoured pseudosuchians from the Upper Triassic continental beds. In S. J. Nesbitt, J. B. Desojo, & R. B. Irmis (Eds.), Antomy, phylogeny and Palaeobiology of early archosaurs and their kin (pp. 203–239). Geological Society.
- Desojo, J. B., & Vizcaíno, S. F. (2009). Jaw biomechanics in the South American aetosaur *Neoaetosauroides engaeus*. *Pal- äontlogische Zeitschrift*, 83, 499–510.
- Dumont, E. R., Grosse, I. R., & Slater, G. J. (2009). Requirements for comparing the performance of finite element models of biological structures. *Journal of Theoretical Biology*, 256, 96–103.
- Dutel, H., Gröning, F., Sharp, A. C., Watson, P. J., Herrel, A., Ross, C. F., Jones, M. E., Evans, S. E., & Fagan, J. (2021). Comparative cranial biomechanics in two lizard species: Impact of variation in cranial design. *Journal of Experimental Biology*, 224, jeb234831.
- Dzemski, G., & Christian, A. (2007). Flexibility along the neck of the ostrich (*Struthio camelus*) and consequences for the reconstruction of dinosaurs with extreme neck length. *Journal of Morphology*, 268, 701–714.
- Erickson, G. M., Gignac, P. M., Steppan, S. J., Lappin, A. K., Vliet, K. A., Brueggen, J. D., Inouye, B. D., Kledzik, D., & Webb, G. J. (2012). Insights into the ecology and evolutionary success of crocodilians revealed through bite-force and toothpressure experimentation. *PLoS One*, 7, e31781.
- Erickson, G. M., Lappin, A. K., & Vliet, K. A. (2003). The ontogeny of bite-force performance in American alligator (*Alligator mississippiensis*). *Journal of Zoology*, 260, 317–327.
- Ferry-Graham, L. A., Bolnick, D. I., & Wainwright, P. C. (2002). Using functional morphology to examine the ecology and evolution of specialization. *Integrative and Comparative Biology*, 42, 265–277.
- Fisher, D. C. (1985). Evolutionary morphology: Beyond the analogous, the anecdotal and the ad hoc. *Paleobiology*, 11, 120–138.
- Galton, M. P. (1985). Diet of prosauropod dinosaurs from the late Triassic and early Jurassic. *Lethaia*, *18*, 105–123.
- Gignac, P. M., & Erickson, G. M. (2017). The biomechanics behind extreme osteophagy in *tyrannosaurus rex. Scientific Reports*, 7, 2012.
- Grigg, G., & Kirshner, D. (2015). Biology and evolution of crocodylians. Cornell University Press.

- Gussekloo, S. W., & Bout, R. G. (2005a). Cranial kinesis in palaeognathous birds. *Journal of Experimental Biology*, 208, 3409–3419.
- Gussekloo, S. W., & Bout, R. G. (2005b). The kinematics of feeding and drinking in palaeognathous birds in relation to cranial morphology. *Journal of Experimental Biology*, 208, 3395–3407
- Heckert, A. B., Lucas, S. G., Rinehart, L. F., Celeskey, M. D., Spielmann, J. A., & Hunt, A. P. (2010). Articulated skeletons of the aetosaur *Typothorax coccinarum* Cope (Archosauria: Stagonolepididae) from the Upper Triassic Bull Canyon Formation (Revueltian: early-mid Norian), easterm New Mexico, USA. *Journal of Vertebrate Paleontology*, 30, 619–642.
- Herring, S. W., & Teng, S. (2000). Strain in the braincase and its sutures during function. American Journal of Physical Anthropology, 112, 575–593.
- Hertel, F. (1995). Ecomorphological indications of feeding behaviour in recent and fossil raptors. *The Auk*, *112*, 890–903.
- Holliday, C. M. (2009). New insights into dinosaur jaw muscle anatomy. The Anatomical Record, 229, 1246–1265.
- Holliday, C. M., Sellers, K. C., Vickaryous, M. K., Ross, C. F., Porro, L. B., Witmer, L. M., & Davis, J. L. (2015). The functional and evolutionary significance of the crocodyliform pterygomandibular joint. *Integrative and Comparative Biology*, 55, e81.
- Holliday, C. M., Tsai, H. P., Skiljan, R. J., George, I. D., & Pathan, S. (2013). A 3D interactive model and atlas of the jaw musculature of *Alligator mississippiensis*. *PLoS One*, 8, e62806.
- Holliday, C. M., & Witmer, L. M. (2007). Archosaur adductor chamber evolution: Integration of muscoskeletal and topological criteria in jaw muscle homology. *Journal of Morphology*, 268, 457–484.
- Iordansky, N. N. (1973). The skull of Crocodilia. In C. Gans & T. S. Parsons (Eds.), Biology of the Reptilia. Academic Press.
- Jasinoski, S. C., Rayfield, E. J., & Chinsamy, A. (2009). Comparative feeding biomechanics of *Lystrosaurus* and the generalized dicynodont *Oudenodon*. The Anatomical Record, 292, 862–874.
- Ji, Q., Norell, M., Makovicky, P. J., Gao, K., Ji, S., & Yuan, C. (2003). An early ostrich dinosaur and implications for ornithomimosaur phylogeny. *American Museum Novitates*, 3420, 1–19.
- Jones, M. E. H., Button, D. J., Barrett, P. M., & Porro, L. B. (2019). Digital dissection of the head of the rock dove (*Columba livia*) using contrast-enhanced computed tomography. *Zoological Letters*, 5, 17.
- Jones, M. E. H., Curtis, N., O'Higgins, P., Fagan, M. J., & Evans, S. E. (2009). The head and neck muscles associated with feeding in Sphenodon (Reptilia: Lepidosauria: Rhynchocephalia). Palaeontologia Electronica, 12, 7A.
- Jones, M. E. H., Gröning, F., Dutel, H., Sharp, A. C., Fagan, M. J., & Evans, S. E. (2017). The biomechanical role of the chondrocranium and sutures in a lizard cranium. *Journal of the Royal Society Interface*, 14, 20170637.
- Kammerer, C. F., Grande, L., & Westneat, M. W. (2006). Comparative and developmental functional morphology of the jaws of living and fossil gars (Actinopterygii: Lepisosteidae). *Journal of Morphology*, 267, 1017–1031.
- Kobayashi, Y., & Lü, J.-C. (2003). A new ornithomimd dinosaur with gregarious habits from the Late Cretaceous of China. *Acta Palaeontologica Polonica*, 48, 235–259.

- Kobayashi, Y., Lu, J.-C., Dong, Z.-M., Barsbold, R., Azuma, Y., & Tomida, Y. (1999). Herbivorous diet in an ornithomimid dinosaur. *Nature*, 402, 480–481.
- Kupczik, K., Dobson, C. A., Fagan, M. J., Crompton, R. H., Oxford, C. E., & O'Higgins, P. (2007). Assessing mechanical function of the zygomatic region in macaques: Validation and sensitivity testing of finite element models. *Journal of Anatomy*, 210, 41–53.
- Labarre, D., Charruau, P., Platt, S. G., Rainwater, T. R., Cedeño-Vázquez, J. R., & González-Cortes, H. (2017). Morphological diversity of the American crocodile (*Crocodylus acutus*) in the Yucatán Pennisula. *Zoomorphology*, 136, 387–401.
- Lauder, G. V. (1995). On the inference of function from structure. In J. J. Thomason (Ed.), *Functional morphology in vertebrate paleontology* (pp. 1–18). Cambridge University Press.
- Lautenschlager, S. (2013). Cranial myology and bite force performance of *Erlikosaurus andrewsi*: A novel approach for digital muscle reconstructions. *Journal of Anatomy*, 222, 260–272.
- Lautenschlager, S. (2016). Reconstructing the past: Methods and techniques for the digital restoration of fossils. *Royal Society Open Science*, *3*, 160342.
- Lautenschlager, S., Brassey, C. A., Button, D. J., & Barrett, P. M. (2016). Decoupled form and function in disparate herbivorous dinosaur clades. *Scientific Reports*, 6, 26495.
- Lautenschlager, S., Bright, J. A., & Rayfield, E. J. (2014). Digital dissection using contrast-enhanced computed tomography scanning to elucidate hard-and-soft-tissue anatomy in the Common Buzzard Buteo buteo. Journal of Anatomy, 224, 412-431.
- Lautenschlager, S., Witmer, L. M., Altangerel, P., & Rayfield, E. J. (2013). Edentulism, beaks, and biomechanical innovations in the evolution of theropod dinosaurs. *Proceedings of the National Academy of Sciences of the United States of America*, 110, 20657–20662.
- Makovicky, P. J., Kobayashi, Y., & Currie, P. J. (2004). Ornithomimosauria. In D. B. Weishampel, P. Dodson, & H. Osmolska (Eds.), *The Dinosauria* (2nd ed., pp. 137–150). University of California Press.
- Massey, F. P., Ennos, A. R., & Hartley, S. E. (2007). Herbivore specific induction of silica-based plant defences. *Plant Animal Interactions*, *152*, 677–683.
- McCurry, M. R., Mahony, M., Clausen, P. D., Quayle, M. R., Walmsley, C. W., Jessop, T. S., Wroe, S., Richards, H., & McHenry, C. R. (2015). The relationship between cranial structure, biomechanical performance and ecological diversity in varanoid lizards. *PLoS One*, 10, e0130625.
- McHenry, C. R., Clausen, P. D., Daniel, W. J. T., Meers, M. B., & Pendharkar, A. (2006). Biomechanics of the rostrum in crocodilians: A comparative analysis using finite-element modeling. *The Anatomical Record*, 288, 827–849.
- Mehl, M. G. (1915). *Poposaurus gracilis*, a new reptile from the Triassic of Wyoming. *The Journal of Geology*, 23, 516–522.
- Milton, S. J., Dean, W. R. J., & Siegfried, W. R. (1994). Food selection by ostrich in South Africa. *Journal of Wildlife Management*, 58, 234–248.
- Moazen, M., Costantini, D., & Bruner, E. (2013). A sensitivty analysis to the role of the fronto-parietal suture in *Lacerta bilineata*: A preliminary finite element study. *The Anatomical Record*, 296, 198–209.

- Moazen, M., Curtis, N., O'Higgins, P., Jones, M. E. H., Evans, S. E., & Fagan, M. J. (2009). Assessment of the role of sutures in a lizard skull: A computer modelling study. *Proceedings of the Royal Society B: Biological Sciences*, 276, 39–46.
- Montefeltro, F. C., Lautenchlager, S., Godoy, P. L., Ferreira, G. S., & Butler, R. J. (2020). A unique predator in a unique ecosystem: Modelling the apex predator within a Late Cretaceous crocodyliform-dominated fauna from Brazil. *Journal of Anatomy*, 237, 323–333.
- Montero, R., Daza, J. D., Bauer, A. M., & Abdala, V. (2017). How common are cranial sesamoids among squamates? *Journal of Morphology*, 278, 1400–1411.
- Nesbitt, S. J. (2003). *Arizonasaurus* and its implications for archosaur divergence. *Proceedings of the Royal Biology B—Biological Sciences*, 270(Supplement 2), S234–S237.
- Nesbitt, S. J. (2007). The anatomy of *Effigia okeeffeae* (Archosauria, Suchia), theropod-like convergence, and the distribution of related taxa. *Bulletin of the American Museum of Natural History*, 302, 1–84.
- Nesbitt, S. J. (2011). The early evolution of Archosaurs: Relationships and the origin of Major Clades. *Bulletin of the American Museum of Natural History*, 352, 1–292.
- Nesbitt, S. J., Liu, J., & Li, C. (2010). A sail-backed suchian from the Heshanggou Formation (Early Triassic: Olenekian) of China. Earth and Environmental Science Transactions of the Royal Society of Edinburgh, 101, 271–284.
- Nesbitt, S. J., & Norell, M. A. (2006). Extreme convergence in the body plans of an early suchian (Archosauria) and ornithomimid dinosaurs (Theropoda). *Proceedings of the Royal Biology B—Biological Sciences*, 273, 1045–1048.
- Norell, M. A., Makovicky, P. J., & Currie, P. J. (2001). The beaks of ostrich dinosaurs. *Nature*, 412, 873–874.
- Osmólska, H. (1997). Ornithomimosauria. In P. J. Currie & K. Padian (Eds.), Encyclopedia of dinosaurs (pp. 499–503). Academic Press.
- Osmólska, H., Roniewicz, E., & Barsbold, R. (1972). A new dinosaur, *Gallimimus bullatus* n. gen., n. sp. (Ornithomimidae) from the Upper Cretaceous of Mongolia. *Palaeontologia Polonica*, *27*, 103–143.
- Parker, W. G., & Martz, J. W. (2010). The Late Triassic (Norian) Adamanian–Revueltian tetrapod faunal transition in the Chinle Formation of Petrified Forest National Park, Arizona. Earth and Environmental Science Transactions of the Royal Society of Edinburgh, 101, 231–260.
- Parker, W. G., & Nesbitt, S. J. (2013). Cranial remains of *Poposaurus gracilis* (Pseudosuchia: Poposauroidea) from the Upper Triassic, the distribution of the taxon, and it simplications for poposauroid evolution. In S. J. Nesbitt, J. B. Desojo, & R. B. Irmis (Eds.), *Anatomy, phylogeny and Palaeobiology of early archosaurs and their kin* (pp. 503–523). The Geological Society.
- Pêgas, R. V., Costa, F. R., & Kellner, A. W. A. (2021) Reconstruction of the adductor chamber and predicted bite force in pterodactyloids (Pterosauria). *Zoological Journal of the Linnean Society*, 193, 602–635.
- Porro, L. B., Holliday, C. M., Anapol, F., Ontiveros, L. C., Ontiveros, L. T., & Ross, C. F. (2011). Free body analysis, beam mechanics, and finite element modelling of the manidble of *Alligator mississippiensis*. *Journal of Morphology*, 272, 910–937.

- Porro, L. B., Metzger, K. A., Iriarte-Diaz, J., & Ross, C. F. (2013). In vivo bone strain and finite element modeling of the manidble of Alligator mississippiensis. Journal of Anatomy, 223, 195–227.
- Rafferty, K. L., Herring, S. W., & Marshall, C. D. (2003). Biomechanics of the rostrum and the role of facial sutures. *Journal of Morphology*, 257, 33–44.
- Rayfield, E. J. (2007). Finite element analysis and understanding the biomechanics and evolution of living and fossil organisms. *Annual Review of Earth and Planetary Sciences*, 35, 541–576.
- Rayfield, E. J. (2011). Strain in the ostrich mandible during simulated pecking and validation of specimen-specific finite element models. *Journal of Anatomy*, 218, 47–58.
- Rayfield, E. J., & Milner, A. C. (2008). Establishing a framework for archosaur cranial mechanics. *Paleobiology*, 34, 494–515.
- Santana, S. E. (2016). Quantifying the effect of gape and morphology on bite force: Biomechanical modelling and in vivo measurements in bats. Functional Ecology, 30, 557–565.
- Santana, S. E., & Dumont, E. R. (2009). Connecting behaviour and performance: The evolution of biting behaviour and bite force performance in bats. *Journal of Evolutionary Biology*, 22, 2131– 2145.
- Santana, S. E., Dumont, E. R., & Davis, J. L. (2010). Mechanics of bite force production and its relationship to diet in bats. *Functional Ecology*, 24, 776–784.
- Schachner, E. R., Irmis, R. B., Huttenlocker, A. K., Sanders, K., Cieri, R. L., & Nesbitt, S. J. (2019). Osteology of the Late Triassic bipedal archosaur *Poposaurus gracilis* (Archosauria: Pseudosuchia) from Western North America. *The Anatomical Record*, 303, 874–917.
- Schwartz, H. L., & Gilette, D. D. (1994). Geology and taphonomy of the *Coelophysis* Quarry, Upper Triassic Chinle Formation, New Mexico. *Journal of Paleontology*, 68, 1118–1130.
- Sellers, K. C., Middleton, K. M., Davis, J. L., & Holliday, C. M. (2017). Ontogeny of bite force in a validated biomechanical model of the American alligator. *Journal of Experimental Biol*ogy, 220, 2036–2046.
- Somaweera, R., Nifong, J., Rosenblatt, A., Brien, M. L., Combrink, X., Elsey, R. M., Grigg, G., Magnusson, W. E., Mazzotti, F. J., Pearcy, A., Platt, S. G., Shirley, M. H., Tellez, M., Van Der Ploeg, J., Webb, G., Whitaker, R., & Webber, B. L. (2020). The ecological importance of crocodylians: Towards evidence-based justification for their conservation. *Biological Reviews*, 95, 936–959.
- Soons, J., Herrel, A., Genbrugge, A., Adriaens, D., Aerts, P., & Dirckx, J. (2012). Multi-layered bird beaks: A finite-element approach towards the role of keratin in stress dissipation. *Journal of the Royal Society Interface*, *9*, 1787–1796.
- Stocker, M. R. (2012). A new phytosaur (Archosauriformes, Phytosauria) from the Lot's Wife beds (Sonsela Member) within the Chinle Formation (Upper Triassic) of Petrified Forest National Park, Arizona. *Journal of Vertebrate Paleontology*, 32, 573–586.
- Stocker, M. R., Nesbitt, S. J., Criswell, K. E., Parker, W. G., Witmer, L. M., Rowe, T. B., Ridgely, R., & Brown, M. A. (2016). A dome-headed stem archosaur exemplifies convergence among dinosaurs and their distant relatives. *Current Biology*, 26, 2674–2680.

- Taborda, J. R. A., Desojo, J. B., & Dvorkin, E. N. (2021). Biomechanical skull study of the aetosaur Neoaetosauroides engaeus using finite element analysis. *Ameghiniana*, *58*, 401–415.
- Tahara, R., & Larsson, H. C. E. (2011). Cranial pneumatic anatomy of *Ornithomimus edmontonicus* (Ornithomimidae: Theropoda). *Journal of Vertebrate Paleontology*, 31, 127–143.
- Thomason, J. J. (1991). Cranial strength in relation to estimated biting forces in some mammals. Canadian Journal of Zoology, 69, 2326–2333.
- Thomason, J. J. (1995). Functional morphology in vertebrate morphology. Cambridge University Press.
- Tsai, H. P., & Holliday, C. M. (2011). Ontogeny of the *Alligator* cartilago transiliens and its significance for sauropsid jaw muscle evolution. *PLoS One*, 6, e24935.
- Walker, A. D. (1964). Triassic reptiles from the Elgin area: Ornithosuchus and the origin of carnosaurs. Transactions of the Royal Society of London, Series B, Biological Sciences, 248, 53–134.
- Walmsley, C. W., Smits, P. D., Quayle, M. R., McCurry, M. R., Richards, H. S., Oldfield, C. C., Wroe, S., Cluasen, P. D., & McHenry, C. R. (2013). Why the long face? The mechanics of mandibular symphysis proportions in crocodiles. *PLoS One*, 8, e53873.
- Webb, M. (1957). The ontogeny of the cranial bones, cranial peripheral and cranial parasympathetic nerves, together with a study of the visceral muscles of *Struthio. Acta Zoologica*, 38, 81–203.
- Weinbaum, J. C. (2011). The skull of *Postosuchus kirkpatricki* (Archosauria: Paracrocodyliformes) from the upper Triassic of the United States. *PaleoBios*, 30, 18–44.
- Weinbaum, J. C. (2013). Postcranial skeleton of *Postosuchus kirkpatricki* (Archosauria: Paracrocodylomorpha), from the upper Triassic of the United States. In S. J. Nesbitt, J. B. Desojo, & R. B. Irmis (Eds.), *Anatomy, phylogeny and Palaeobiology of early archosaurs and their kin* (pp. 525–553). Geological Society.
- Williams, J. B., Siegfried, W. R., & Milton, S. J. (1993). Field metabolism, water requirements and foraging behaviour of wild ostriches in the Namib. *Ecology*, 74, 390–404.
- Witmer, L. M., & Ridgely, R. C. (2008). The paranasal air sinuses of predatory and armored dinosaurs (Archosauria: Theropoda and Ankylosauria) and their contribution to cephalic structure. *The* Anatomical Record, 291, 1362–1388.
- Witzmann, F., Schwarz-Wings, D., Hampe, O., Fritsch, G., & Asbach, P. (2014). Evidence of spondyloarthopathy in the spine of a phytosaur (Reptilia: Archosauriformes) from the Late Triassic of Halberstadt, Germany. *PLoS ONE*, *9*, e85511.

- Xu, X., Clark, J. M., Mo, J., Choiniere, J. N., Forster, C. A., Erickson, G. M., Hone, D. W. E., Sullivan, C., Eberth, D. A., Nesbitt, S. J., Zhao, Q., Hernandez, R., Jia, C.-K., Han, F.-L., & Guo, Y. (2009). A Jurassic ceratosaur from China helps clarify avian digital homologies. *Nature*, 459, 940–944.
- Young, M. T., Rayfield, E. J., Holliday, C. M., Witmer, L. M., Button, D. J., Upchurch, P., & Barrett, P. M. (2012). Cranial biomechanics of *Diplodocus* (Dinosauria, Sauropoda): Testing hypotheses of feeding behaviour in an extinct megaherbivore. *Naturwissenschaften*, 99, 637–643.
- Zanno, L. E., & Makovicky, P. J. (2011). Herbivorous ecomorphology and specialization patterns in theropod dinosaur evolution. Proceedings of National Academy of Sciences of United States of America, 108, 232–237.
- Zapata, U., Metzger, K. A., Wang, Q., Elsey, R. M., Ross, C. F., & Dechow, P. C. (2010). Material properties of mandibular cortical bone in the American alligator, *Alligator mississipiensis*. *Bone*, 46, 860–867.
- Zhang, F. K. (1975). A new thecodont *Lotosaurus*, from the Middle Triassic of Hunan. *Vertebrata PalAsiatica*, 13, 144–147.
- Zusi, R. (1993). Patterns of diversity in the avian skull. In J. Hanken & B. K. Hall (Eds.), *The Skull*. University of Chicago Press.
- Zweers, G., Bout, R., & Heidweiller, J. (1994). Motor organization of the avian head-neck system. In M. N. O. Davies & P. R. Green (Eds.), *Perception and motor control in birds* (pp. 201–221). Springer.

SUPPORTING INFORMATION

Additional supporting information may be found in the online version of the article at the publisher's website.

How to cite this article: Bestwick, J., Jones, A. S., Nesbitt, S. J., Lautenschlager, S., Rayfield, E. J., Cuff, A. R., Button, D. J., Barrett, P. M., Porro, L. B., & Butler, R. J. (2021). Cranial functional morphology of the pseudosuchian *Effigia* and implications for its ecological role in the Triassic. *The Anatomical Record*, 1–28. https://doi.org/10.1002/ar.24827